5G Communication with a Heterogeneous, Agile Mobile network in the Pyeongchang Winter Olympic competition

Grant agreement n. 723247

Deliverable D6.3
Integration and system testing phase of satellite scenario

Date of Delivery:	31 May 2018	31 May 2018 (Actual)
Editor:	T. Deleu	
Associate Editors:	B. Vautherin	
Authors:	Jani Saloranta, Benoît Vautherin, Roc Maymo-Camps, Jean-Baptiste Doré, Raffaele D'Errico, M. Gineste, T.Deleu	
Dissemination Level:	PU	
Security:	Public	
Status:	Final	
Version:	V1.0	
File Name:	D6.3 - Integration and system testing phase of satellite scenario	
Work Package:	5GCHAMPION_D6.3 _Final	

Modifications	Date	Version
Initial document	31/05/17	1.0

Abstract

This document is related to task 6.3, and provides integration and testing results for satellite communication via 5G radio interfaces as well as positioning performance resulting from GNSS-PPP and 5G positioning techniques. For satellite communications, a 5G radio access network has been emulated with a typical non-geostationary satellite channel, including high Doppler drift. For positioning, software and hardware components related to GNSS-PPP were developed, with a TPZF server providing PPP corrections with log 5G and GNSS returned positions into the location server.

Index terms

5G, satellite communications, GNSS, single positioning, precise point positioning

Contents

1 Introduction

This deliverable provides description of the physical integration results of satellite communication and positioning systems. The deliverable also provides 5G radio and satellite interworking testing with physical integration of different positioning technologies specified by WP5.

1.1 Applicable and reference documents

1.1.1 Applicable documents

Doc	Ref	Date	Version
[GA]	Grant Agreement-723247-5G CHAMPION		

1.1.2 Reference documents

Doc	Ref	Date	Version
[RD0]	RTKLIB ver. 2.4.2 Manual	April 29, 2013	

1.2 Recall of Task 6.3

As stated in [GA] task 6.3 can be divided into two sub tasks.

First “subtask aim at delivering: (i) Implementation of the specified demonstration using existing 5G radio access test bed and (ii) Evaluation of the networking performance of the possible 5G radio interfaces in satellite context through the use of a simplified real time 5Gradio access network test bed including 5G transmitter and receiver implementing the targeted waveforms (NB-IOT and potentially others) and channel emulator implementing the defined satellite channel model.”

Second “subtask aims at delivering: (i) Development and integration of all the software and hardware components related to GNSS-PPP techniques, (ii) Development and integration of all the software and hardware component related to 5G positioning techniques, (iii) Communication to the TPZF server to provide PPP corrections, and log 5G and GNSS returned positions into the location server, and tools to assess their accuracy and (iv) demonstration of the 5G-GNSS interoperability for accurate positioning in indoors and outdoors (in Oulu).”

2 Seamless access for 5G devices to satellite communications

2.1 Notations

Bold letters denote vectors and matrices. Upper-case and lower-case letters denote frequency domain and time domain variables respectively. The following notations were used:

- $(.)^t$ Transpose
- $(.)^H$ Hermitian transform
- $E[.]$ Expectation operator
- $tr(.)$ Trace operator
- $||.||^2$ l²-norm

$\boldsymbol{F}$ stands for the DFT (Discrete Fourier transform) matrix defined as:

$$\boldsymbol{F} = \frac{\mathbf{1}}{\sqrt{\boldsymbol{N}}}\begin{bmatrix} 1 & 1 & 1 & \dots & 1 \\ 1 & W_N^1 & W_N^2 & \dots & W_N^{N-1} \\ \dots & \dots & \dots & & \\ 1 & W_N^{N-1} & W_N^{2(N-1)} & & W_N^{(N-1)(N-1)} \end{bmatrix}$$

where $W_N^1 = \mathrm{e}^{\mathrm{j}\frac{2\pi}{N}}$

2.2 Testbed configuration

2.2.1 Doppler simulation

In recent years, there have been several proposals to use networks of satellites in Low-Earth-Orbits (LEO) for communications. LEO satellites can be selected to supplement terrestrial networks by providing connectivity to area in which providing a terrestrial link is difficult or too expensive.

The use of LEO satellites has an advantage with respect to Geosynchronous Earth-Orbits (GEO) satellites: the round trip delay is shorter. Typically, LEO satellite orbits are 1500 km and the round trip delays are less than 10ms. However, the low altitude also introduces disadvantages including short orbit periods, more satellites to provide full coverage of the earth and a high relative velocity experienced at earth.

The channel between the earth and the satellite can be modeled by a geometric method, i.e ray - tracing. Knowing the elevation, the velocity and the orbit of the satellite, the amplitude and phase of the direct ray can be easily expressed. As an example, we have depicted in Figure 1 the variation of the satellite elevation as well as the Doppler frequency for a carrier frequency of 1.2 GHz (satellite altitude of 800 km).

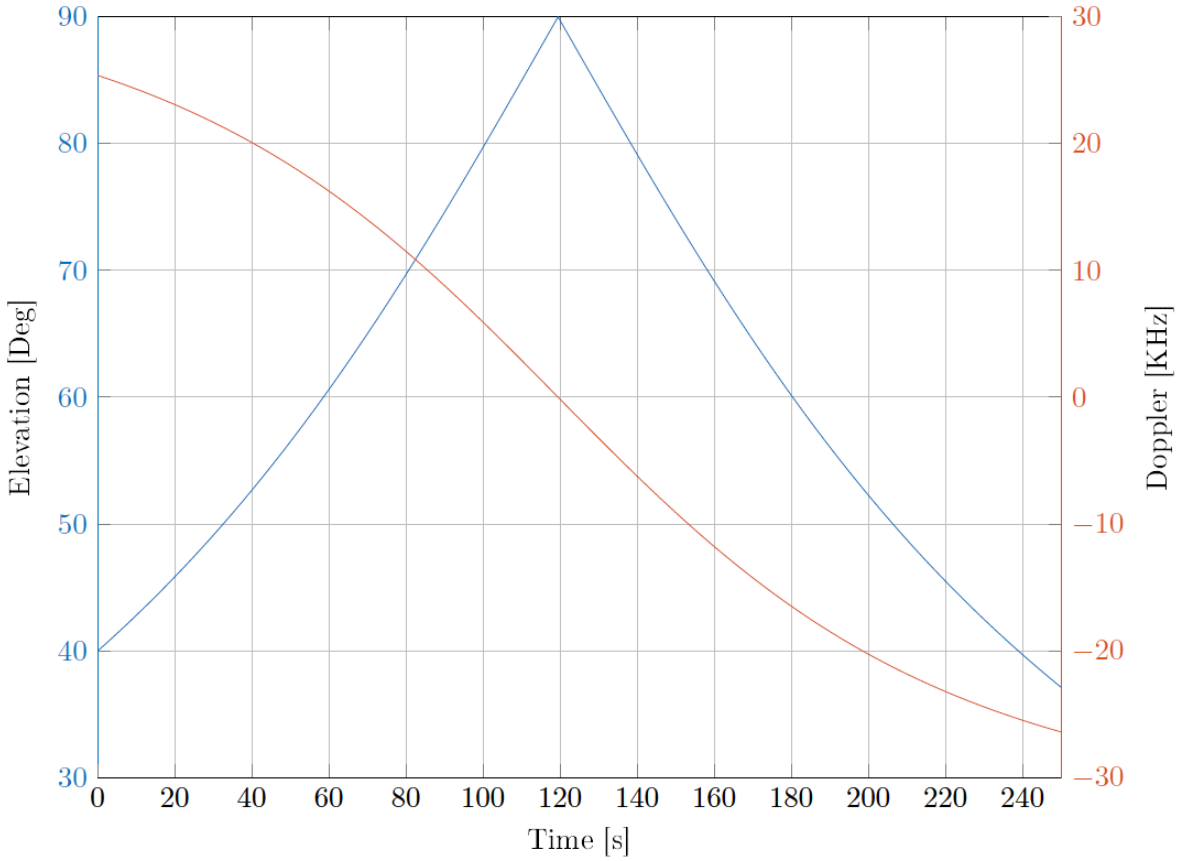

Figure 1 - Doppler frequency and satellite elevation angle versus time.

We clearly see that the Doppler frequency can be strong, up to 30 kHz. Now, if we consider a transmission of few ms, typically 10-100 ms, the Doppler frequency is seen by the receiver as a constant frequency shift, i.e a Carrier Frequency Offset (CFO) as well as a small variation of the Doppler frequency. From the physical layer perspective, it is required to design a robust synchronization procedure able to manage a large CFO as well as an efficient channel estimation algorithm to track the frequency Doppler variation.

2.2.2 Channel estimation

One advantage of OFDM waveform over single carrier modulation is a simplified equalization procedure. As long as the duration of the channel impulse response is shorter than the guard interval and the channel is constant over the duration of the OFDM symbol, a frequency-selective wideband channel converts to a number of sub-carriers channel with flat fading.

In this work, we propose a three steps channel estimation procedure. Firstly, a least square (LS) estimation on pilot sub-carriers is performed. Secondly, a de-noising filtering is done for each symbol based on the N_a LS estimates. Thirdly, a time interpolation is realized.

First, let's describe how the de-noising filtering is realized. Accurate estimation, of the channel coefficients H[f] may be derived from the observation of P[f] using a filter W_f. To construct the filter W_f, the following minimization problem should be solved:

$$\underset{\mathbf{W_f}}{argmin} E[||\mathbf{W_f P} - \mathbf{H}||^2]$$

Let Ω be defined as:

$$\Omega = E[||\mathbf{W_f P} - \mathbf{H}||^2]$$

Then, since **P** is a least square estimate of the pilot sequence, the following equation may be written:

$$\mathbf{P} = \mathbf{H} + \mathbf{N}$$

where **N** is a N_a x 1 noise vector. Equation may then be rewritten as:

$$\begin{aligned} \Omega &= E[||\mathbf{W_f}(\mathbf{H}+\mathbf{N}) - \mathbf{H}||^2] \\ &= E[tr[\mathbf{W_f H H}^H \mathbf{W_f}^H - \mathbf{W_f H H}^H - \mathbf{H H}^H \mathbf{W_f}^H + \\ &\quad \mathbf{H H}^H + \mathbf{W_f N N}^H \mathbf{W_f}^H]] \end{aligned}$$

Then, if **h** is the N_{FFT} x 1 vector of the channel impulse response, **H** may be written as:

$$\mathbf{H} = \mathbf{F}(\mathbf{1}:\mathbf{N_a}, :)\mathbf{h} = \mathbf{F_{N_a}}\mathbf{h}$$

Finally we can write:

$$\begin{aligned} \Omega &= tr[\mathbf{W_f F_{N_a}} \mathbf{\Phi_h} \mathbf{F_{N_a}}^H \mathbf{W_f}^H - \mathbf{W_f F_{N_a}} \mathbf{\Phi_h} \mathbf{F_{N_a}}^H \\ &\quad - \mathbf{F_{N_a}} \mathbf{\Phi_h} \mathbf{F_{N_a}}^H \mathbf{W_f}^H + \mathbf{F_{N_a}} \mathbf{\Phi_h} \mathbf{F_{N_a}}^H \\ &\quad + \mathbf{W_f R_N W_f}^H] \end{aligned}$$

where $\mathbf{\Phi_h}$ is the time domain channel autocorrelation matrix of size N_{FFT} x N_{FFT} and $\mathbf{R_N}$ is the noise autocorrelation matrix. By taking the partial derivative of Ω with respect to $\mathbf{W_f}$ and making it equal to zero, it becomes:

$$\begin{aligned} \frac{\partial \Omega}{\partial \mathbf{W_f}} &= 0 \\ 0 &= (\mathbf{\Delta} + \mathbf{R_N})\mathbf{W_f}^H - \mathbf{\Delta} \\ \mathbf{W_f}^H &= (\mathbf{\Delta} + \mathbf{R_N})^+ \mathbf{\Delta} \end{aligned}$$

Where $\mathbf{\Delta} = \mathbf{F_{N_a}} \mathbf{\Phi_h} \mathbf{F_{N_a}}^H$. When pilots with constant amplitude are sent then the noise distribution after LS estimation is the same for each sample and therefore $\mathbf{R_N} = \sigma_n^2 \mathbf{I}$ with σ_n^2 the variance of the noise. However, if noisy-pilots are transmitted, then the amplitude of each pilot differs from one to another. Consequently the statistic of the noise after LS estimation varies and in that case, $\mathbf{R_N} = \sigma_n^2$ $\mathbf{R_{NZ}}$ where $\mathbf{R_{NZ}}$ (i,j) = 0 when i≠ j, $||\mathbf{Z}(i) + \mathbf{X}(i)||^{-2}$ otherwise.

The question, then, is how the performance of the filter is impacted by the introduction of the noisy-pilots scheme. For that performance of the proposed channel estimation scheme has been assessed for two cases, constant amplitude pilots and noisy-pilots. We assume a FFT size of 128 points and N_a = 32 sub-carriers and a perfect knowledge of the channel statistics, i.e $\mathbf{\Phi_h}$. Figure 2 depicts the performance of the denoising filter for a single tap (card(**h**)=1) and a 8-taps channels (card(**h**) =8) with mutually independent Rayleigh distributed coefficients. The relative mean square error (RMSE) of the estimation with respect to the noise free channel coefficient is evaluated for various SNR. The performance is estimated

numerically. In case of noisy-pilots scheme, we consider the sequence optimized for a ρ = 7dB. We also depict the performance of the Zero Forcing (ZF) filter. It should be mentioned that in case of the one tap channel, the ZF estimator is a Maximum Ratio Combining (MRC) filter.

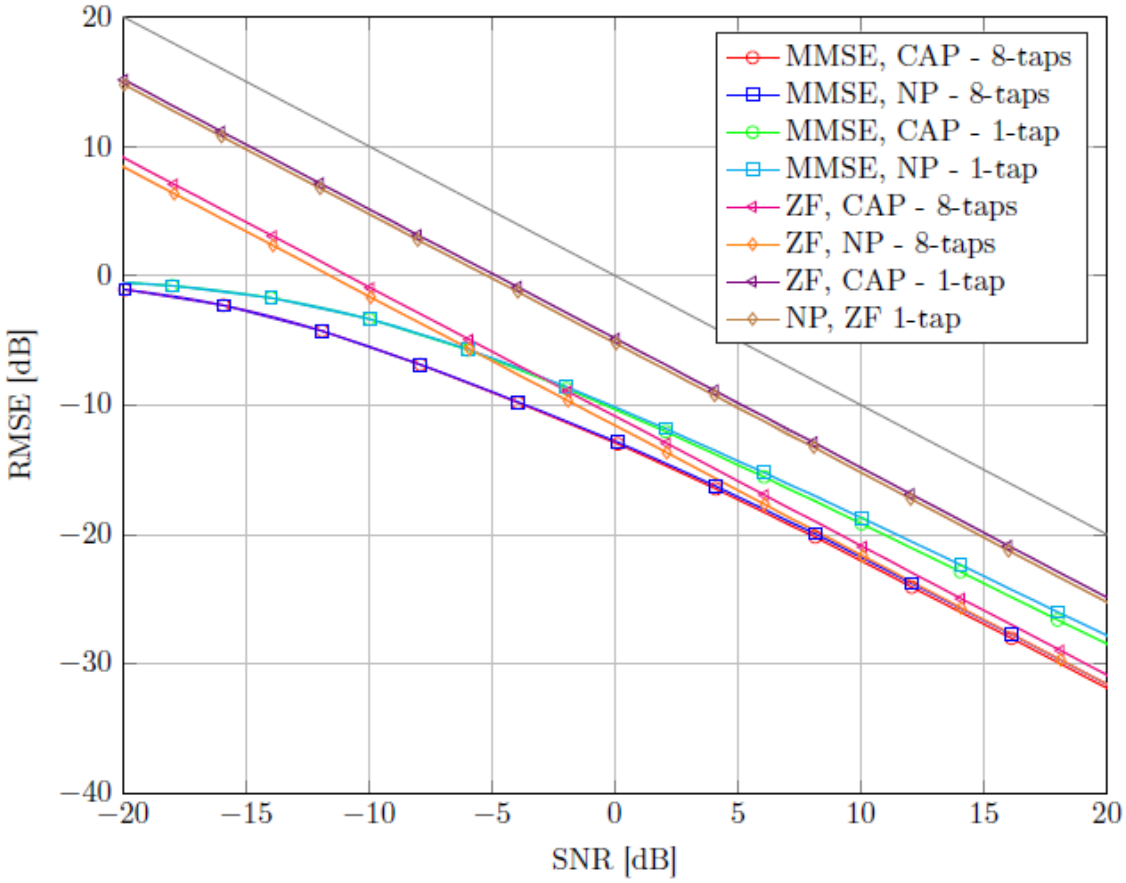

Figure 2 - RMSE versus SNR for different filter and channel. CPA stands for Constant Amplitude Pilots and NP Noisy-Pilots.

The RMSE is below the noise level and better performance is achieved when the channel is flat, i.e 1-tap. As expected the MMSE criterion gives better results at low SNR with respect to ZF. Now if we analyze the difference between the two pilot schemes, the use of noisy-pilots

only introduces a small degradation. We depict in Figure 8

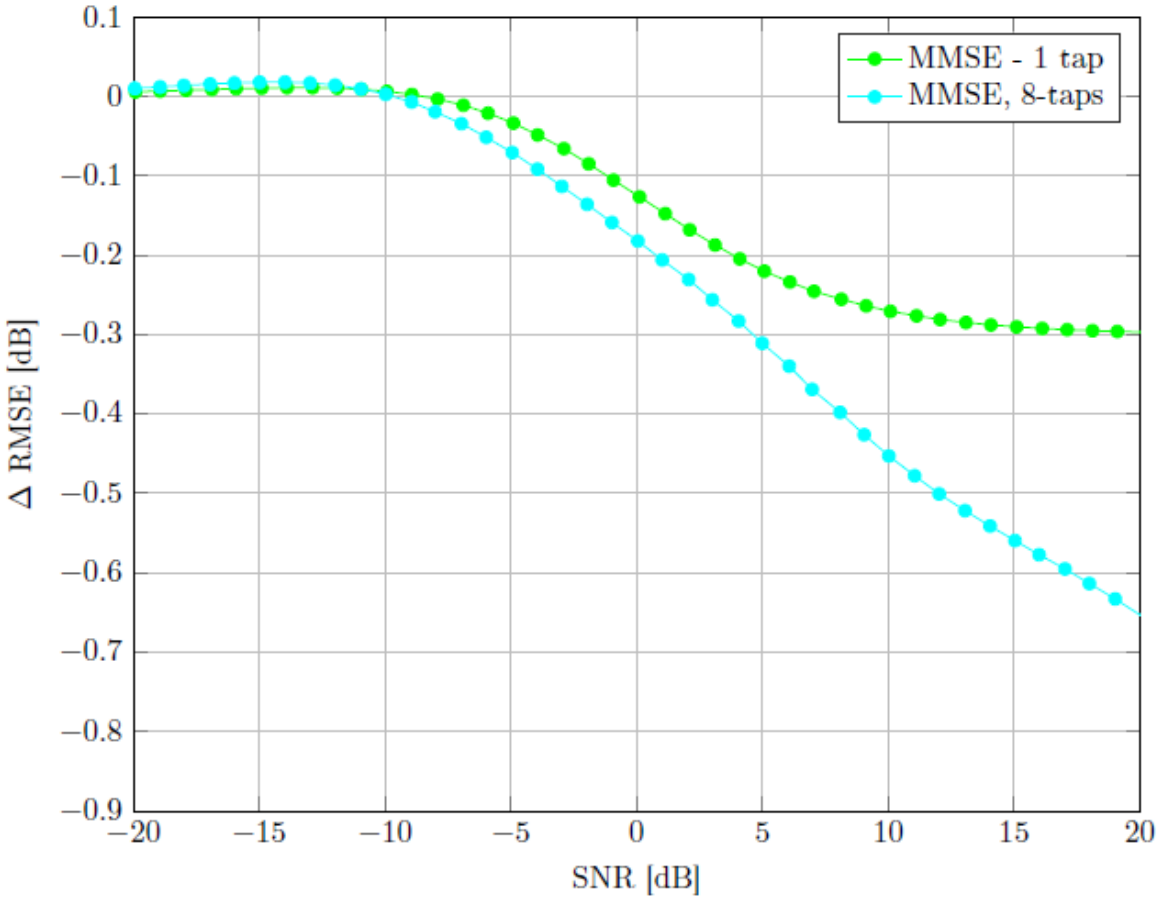

Figure 3the RMSE difference between the two schemes. When the SNR is high, the gap is less than 0.3dB for the 1-tap channel and up to 0.9dB for the 8-taps channel. However in the range of SNR of interest, i.e -10 to 5dB the gap is limited to few tens of dB. It makes the proposed noisy-pilots scheme particularly interesting for the satellite use case (flat channel).

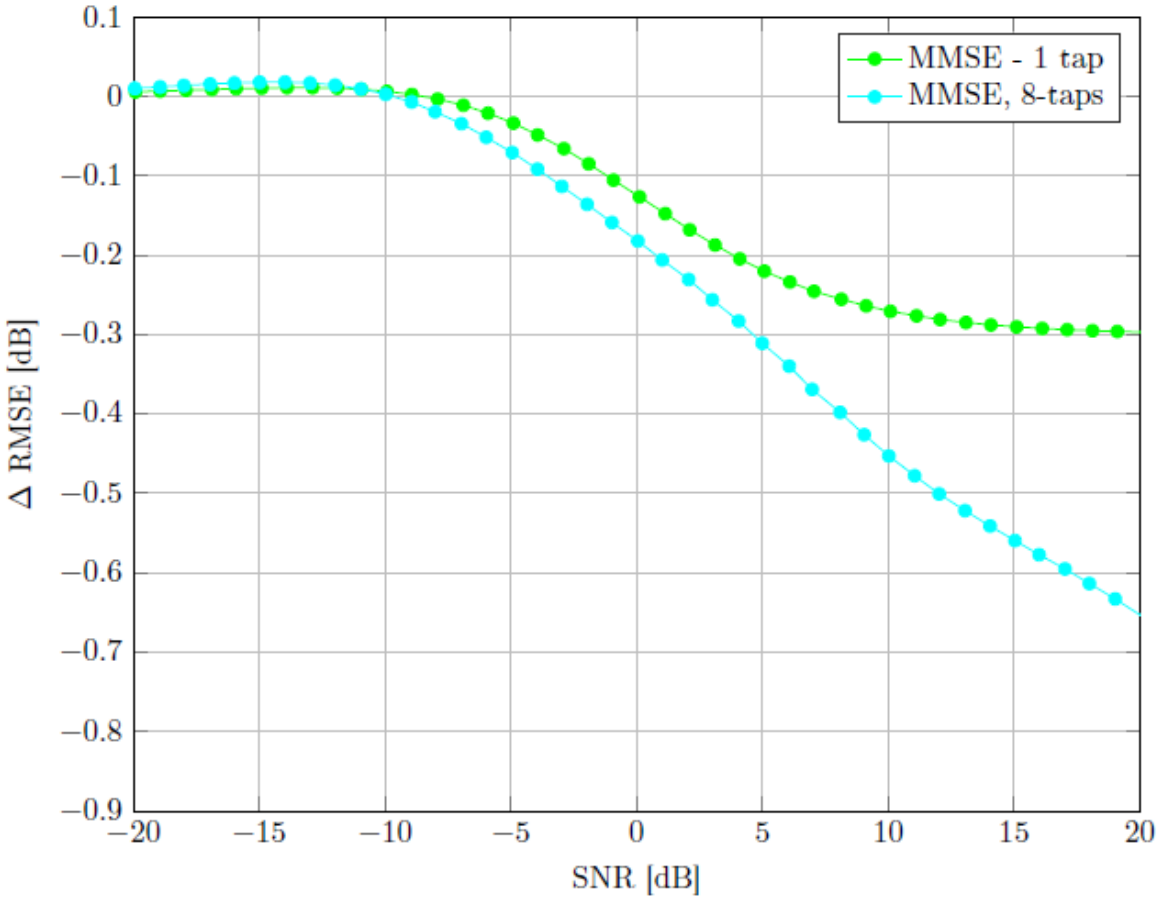

Figure 3 -RMSE loss of two estimator with respect to perfect channel estimation.

Once the channel coefficient has been estimated at each pilot location, a time interpolation filter is applied. In case of satellite channel the channel is characterized by significant Doppler shift. On the scale of a transmitted packet, the Doppler shift is seen as a CFO. Therefore a residual Doppler needs to be tracked by the receiver. As introduced by the authors of [EW2014], we propose to implement a classical Wiener interpolation filter. The challenge is to determine the statistic of the channel covariance matrix. One option is to numerically evaluate the expectation of the covariance matrix along the trajectory of the satellite. The best solution, is to define a set of filter optimized for a set of position. As mentioned previously, the estimation of the CFO gives information on the experienced Doppler shift and therefore an appropriate interpolation filter can be selected. However this method is more complex and requires that the CFO, due to oscillator misalignment is negligible when compared to the Doppler shift. For the rest of the paper, we assume that only one filter is used, with a co-variance matrix estimated by averaging the channel statistic over the trajectory of the satellite.

We have discussed how the channel coefficients can be estimated from LS estimation. The question is now how to determine the parameter D and what is the implementation loss introduced by the proposed scheme. These two questions are addressed in the next subsection.

2.2.3 Pilot density dimensioning

Dimensioning the pilot density is not straightforward. Based on the frame structure discussed in D5.2, we have evaluated the performance of the receiver in two cases, AWGN channel and LEO channel by Monte-Carlo simulations. We consider a Coplanar-Turbo-FSK with $\lambda = 4$ and a bandwidth composed of 32 sub-carriers. For these two channels, we have estimated the SNR to achieve a PER of 10^{-2} for various number of pilot density. Pilot density is managed by setting D from 2 to 12. For each value of D, we have computed the performance loss between a genie aided receiver with a perfect knowledge of the channel[1] and a receiver implementing the LS channel estimation, frequency de-noising as well as time interpolation. Firstly we have estimated the loss based on the SNR. Secondly, the loss is evaluated taking into account the pilot density, i.e. based on the Eb/N0, the Energy per information bit to noise power spectral density ratio. The correction factor to apply to the SNR loss is :

$$10\log_{10}(\frac{D-1}{D})$$

The larger the density of pilot, the better is the channel estimation but the larger is the spectral efficiency penalty. Therefore a trade-off needs to be identified.

We depict in Figure 4, the results for an AWGN channel and in Figure 5 simulation results for the LEO channel defined previously. For this last case, we have assumed that the receiver is able to compensate the Doppler shift experienced at the beginning of the frame. We have simulated a case where the Doppler shift is processed as a CFO by a genie-aided synchronization function. Though, the channel coefficient varies within the frame.

For each value of D, two packet sizes (1024 and 256 bits) and two PSK modulation orders (4 and 32) are simulated. When the packet size is small and the modulation order is large, the number of FFT symbol is small. Consequently, the number of pilots sub-carriers available for channel estimation is reduced.

First, let's describe the results on AWGN channel. First of all, it is obvious that the smaller D, the smaller is the loss regarding the SNR. In case of D=4, the loss is less than 0.5dB for D=4 and D=6 when the payload is 1024 bits. If the size of payload is set to 256 with a 32-PSK, then one can expect 1.2dB loss. In this case the frame is short and the number of pilot distributed within the frame is not sufficient. This effect is highlighted when D=12. In that case the loss is greater than 4.5dB. Now if we compare the loss regarding Eb/N0, the best trade-off is to set D equals to 6. Whatever the configuration, the loss, regarding Eb/N0, is minimized when D=6.

[1] The receiver has a perfect knowledge of the channel coefficient for a given sub-carrier.

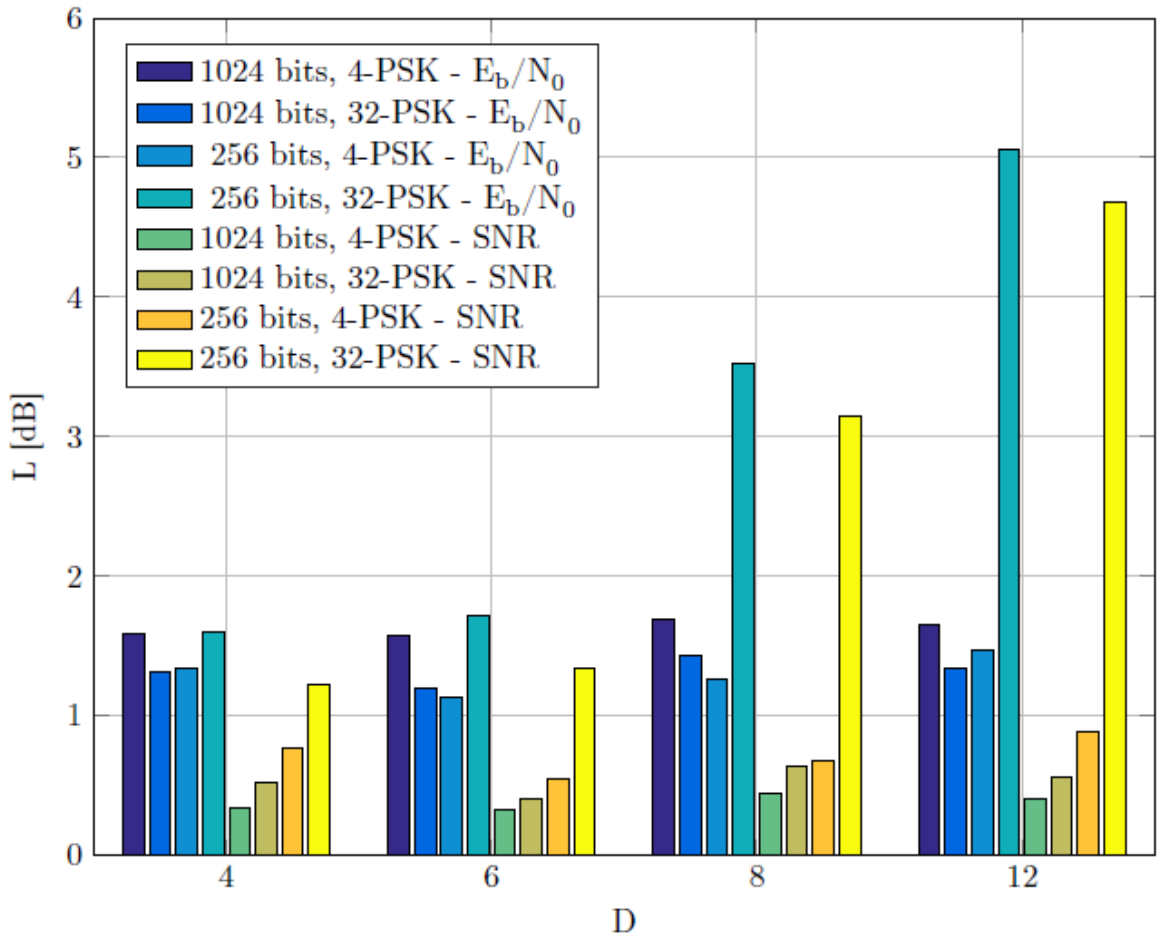

Figure 4 - Performance loss between a genie aided receiver with a perfect knowledge of the channel and the proposed receiver for various pilot density on an AWGN channel.

In case of LEO channel, the results remain almost unchanged. The best trade-off is when D=6. When D=6 the loss is less than 0.5 for all the case excepted when the size of the payload is 256 bits and a 32-PSK signaling is considered.

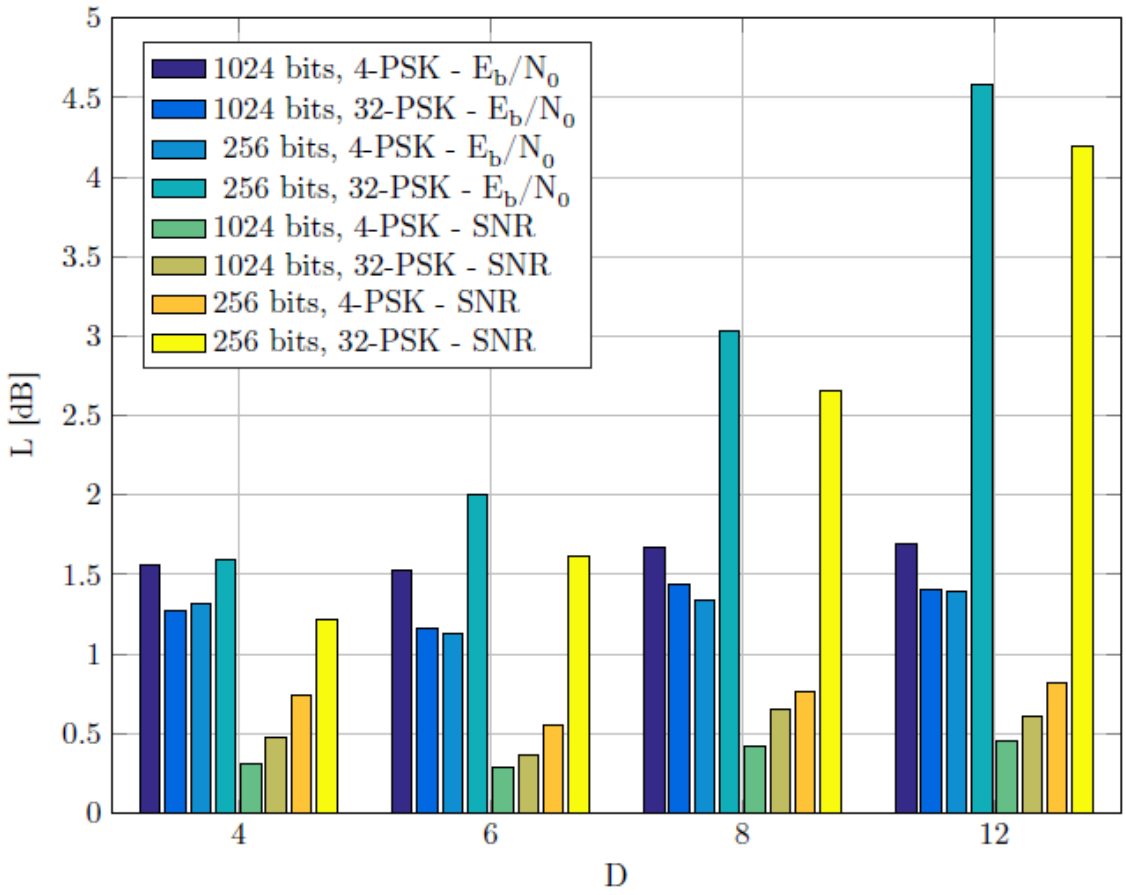

Figure 5 -Performance loss between a genie aided receiver with a perfect knowledge of the channel and the proposed receiver for various pilot density on an LEO channel.

This latest case is particularly challenging. We have to deal with a very short frame, and consequently a limited number of pilots sub-carriers. The estimation of the channel cannot be accurate enough to have good performance. Increasing the pilot density will definitely give better performance regarding SNR. However, the penalty regarding Eb/N0 will increase mechanically.

To conclude, the use of a density of pilot characterized by D=6 is a good trade-off. In that case, for a typical payload of 1024 bits the loss regarding SNR is less than 0.5dB with respect to a genie-aided receiver.

2.3 Platform overview

The platform is composed of a custom digital board and an off-the-shelf radio frequency (RF) transceiver.

The custom digital board is based on the Zynq-045 Xilinx FPGA which integrates a dual Cortex-A9 ARM processor. The block diagram of the FLEX system is shown in Figure 6. The high computational base band processing is implemented in the programmable logic while the ARM processor manages non real time algorithms, external components (RF) as well as Media Access Control (MAC) interfaces. A dedicated Linux environment was also built. Ethernet PHY/MAC is provided for easy local area network (LAN) connectivity. The on-board USB On-The-Go (OTG) gives another connectivity option particularly useful to interact with personal computers or other personal devices. The custom digital board has a reduced size (110 x 75 mm²).

The RF transceiver board is based on the AD9361 component from Analog Device [AD9361]. It is a high performance, highly integrated radio frequency (RF) Agile Transceiver which combines an RF front end with a flexible mixed-signal baseband section. It supports a dual transmitter and a dual receiver with integrated frequency synthesizers. The AD9361 operates in the 70 MHz to 6 GHz range, covering most licensed and unlicensed bands. Channel bandwidths from 200 kHz to 56 MHz are supported.

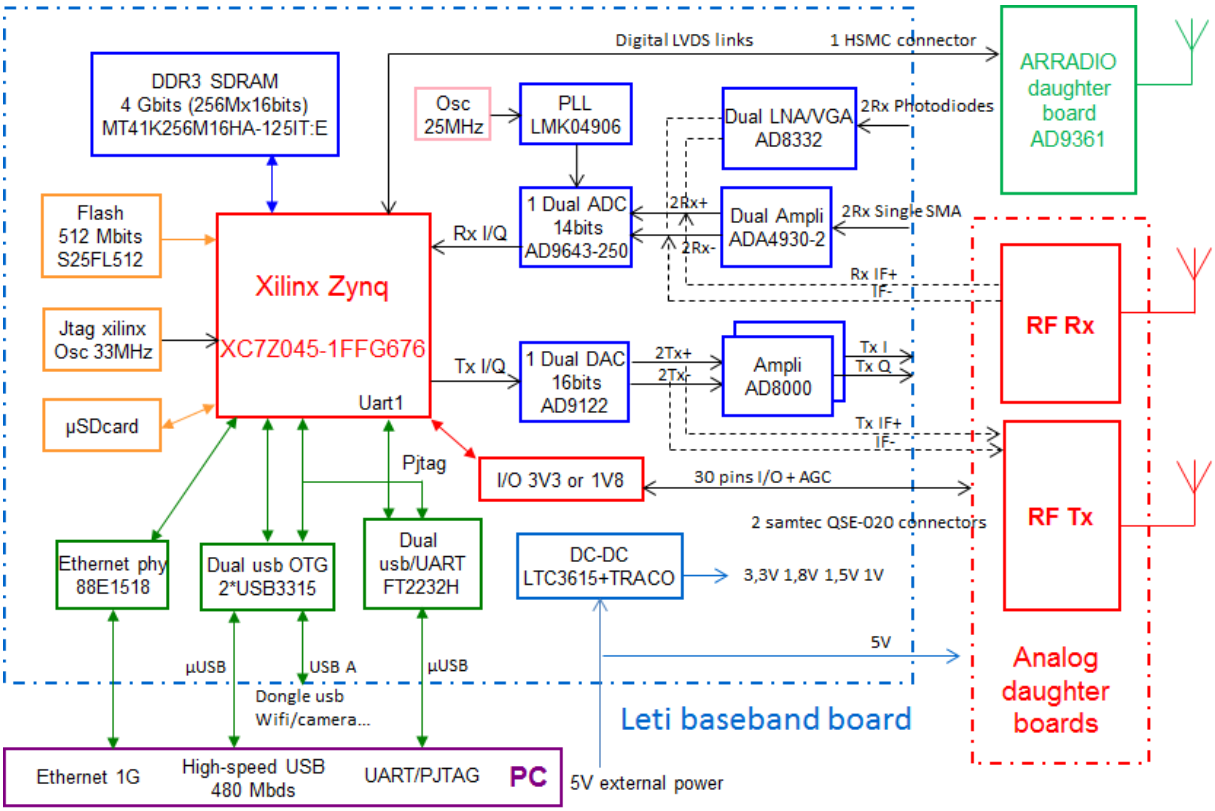

Figure 6 - FLEX board architecture.

2.4 Link-level Performance

This section is dedicated to assess the performance of the Coplanar-Turbo-FSK scheme. First, the performances are numerically evaluated by Monte-Carlo simulations for various

parametrization of the Coplanar-Turbo-FSK. In a second time, the performances are evaluated with a hardware platform, in which some parts of the receiver are implemented.

2.4.1 Monte Carlo simulations

Based on the receiver structure described previously, we have assessed the performance the proposed scheme over the LEO satellite channel at 1.5GHz for various payload sizes, 256 and 1024 bits and four PSK modulations, 2,4,8,16 and 32-PSK using D=6. The required SNR in the useful bandwidth (180 kHz) is evaluated to reach a PER of 0.1. The Coplanar-Turbo-FSK is configured with $\lambda = 4$. The inter carrier spacing is set to 5.625 kHz (32 actives sub-carriers). The throughput varies in the range 8 to 13kbit/s. Once again, we have assumed that the receiver is able to compensate the Doppler shift experienced at the beginning of the frame. We have simulated a case where the Doppler shift is processed as a CFO by a genie-aided synchronization function.

Results are depicted in Figure 7. First, these results clearly highlight that the noisy-pilots scheme considered to reduce the PAPR does not affect the performance. The same performances are achieved with a noisy-pilots scheme with $\rho = 7$dB and $\rho = 20$dB; the difference is lower than 0.03dB.

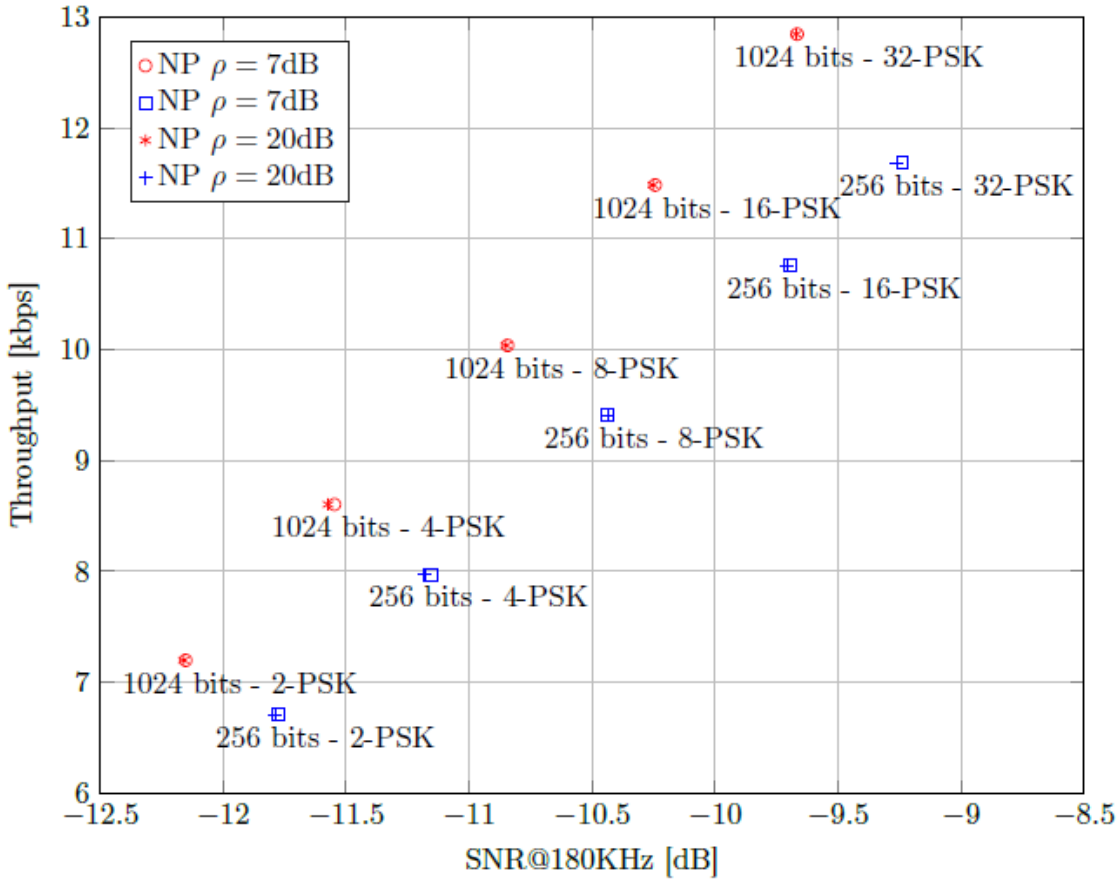

Figure 7 - Performance comparison of Coplanar-Turbo-FSK with 32 sub-carriers and M-PSK, M={2,4,8,16,32}, $\lambda = 4$ = a LEO channel at 1.5GHz.

For the low throughput configuration, a PER of 10^{-1} is reached at a SNR of -10.97dB (SNR computed in a bandwidth of 180 kHz) for 256 bits of payload and -11.42dB for 1024 bits. In case of higher throughput, the working SNR is -9.02dB for 256 bits and -9.58dB for 1024 bits.

2.4.2 Measured performance

For the experimental tests, we have used a channel emulator from Anite. This equipment emulates characteristics of real-world radio channel conditions within a laboratory environment. A LEO channel model has been implemented at a carrier frequency of 1.5GHz. The transmitter is plugged to the channel emulator. Additive White Noise is added to the signal filtered by the LEO channel as depicted in the schematic diagram Figure 8.

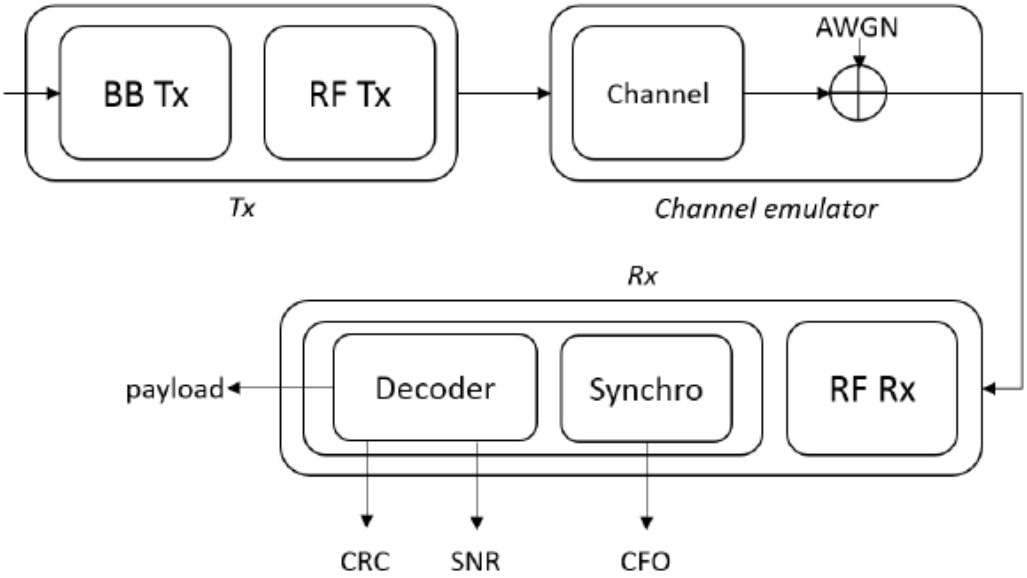

Figure 8 - Schematic diagram of the measurement testbed.

The automatic gain control of the RF Rx has been adjusted and frozen to give the best noise factor when a frame is received. Conversely to the performance assessed by numerical simulations, the synchronization procedure has (i) to detect the beginning of a frame as well as (ii) to compensate the Doppler shift, experienced as a CFO, based on an estimation performed on the preamble of size P=32 symbols. At the receiver side (Baseband BB), the CFO, SNR as well as the state of the CRC (Control Redundancy Check) is computed.

First, we have evaluated the CFO seen by the receiver and estimated by the synchronization procedure. As mentioned previously, at the scale a frame, the Doppler shift is viewed as a CFO. We have illustrated in Figure 9, the estimated CFO in case of a LEO channel at 1.5GHz and a SNR of -8dB (computed in the useful bandwidth, i.e. 180kHz) .

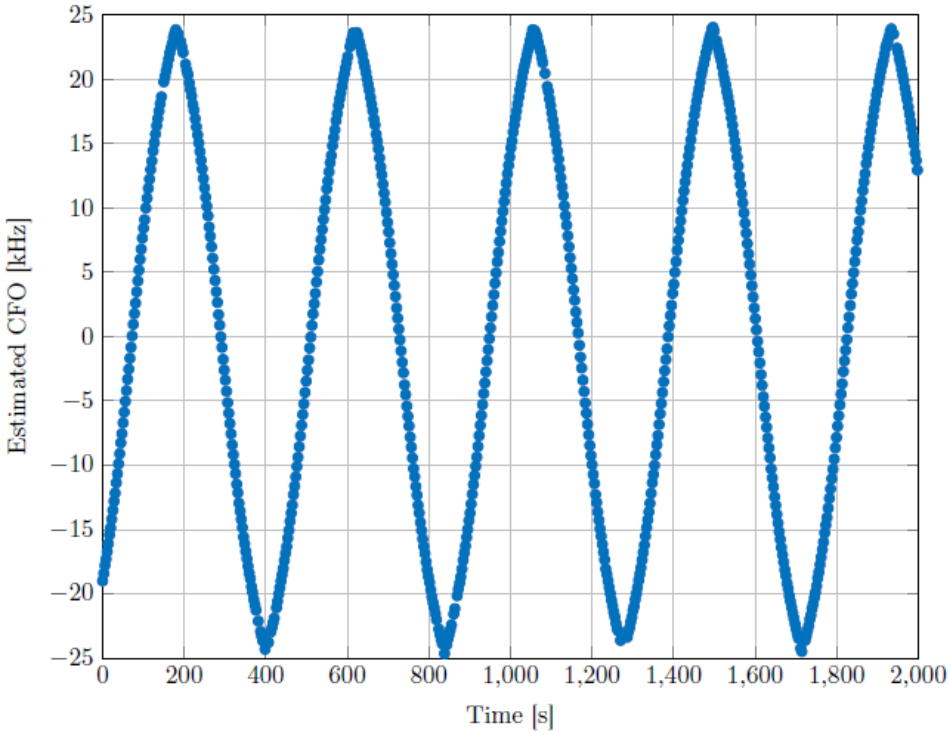

Figure 9 - CFO estimated by the synchronization procedure in case of a LE0 channel at 1.5GHz.

The estimated CFO follows the Doppler shift values, depicted in Figure 1. A shift is introduced by the frequency offset introduced by the RF board.

Similarly to the numerical simulation, we have assessed, for various throughput, the SNR required to reach a packet error rate of 0.1. The detection of an erroneous packet is realized by checking the CRC (16 bits). Experimental results are depicted in Figure 10 .

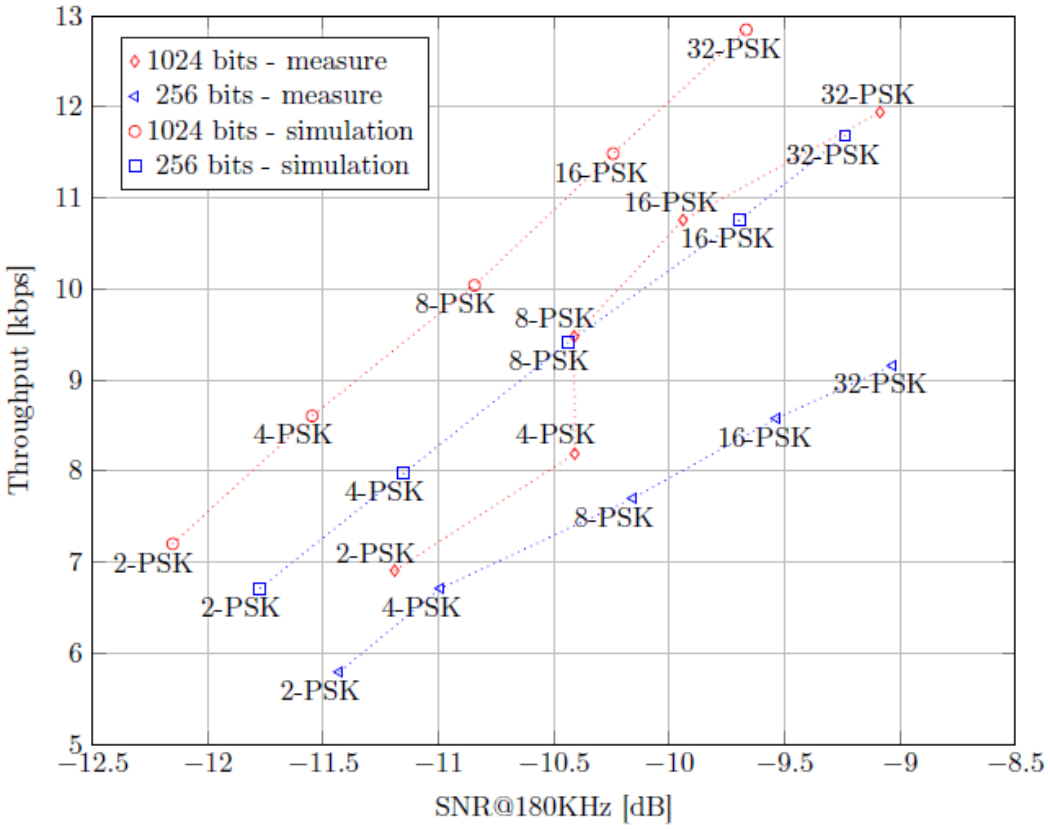

Figure 10 - Performance comparison of Coplanar-Turbo-FSK with 32 sub-carriers and M-PSK, M={2,4,8,16,32}, $\lambda = 4$ for a LEO channel at 1.5GHz with a preamble of size P=32 .

First of all, the required SNR to reach a packet error rate of 0.1 has been computed based on the estimation of the SNR blindly done at the baseband level of the receiver. Therefore, the given figures of merits do not take into account the noise figure of the RF front end. We have measured a noise factor of 1.5 dB that need to be considered for link level estimation. The calibration of the SNR estimator has demonstrated a precision of the estimation of 0.1 dB.

In case of a short payload size (256 bits), the implementation loss is less than 0.25dB. One can noticed that the throughput is reduced due the insertion of the preamble. In case of a short packet (32-PSK), the duration of the preamble is 20% of the total duration.

For the case of a packet size of 1024 bits, the implementation loss is higher, 0.5 to 0.75dB. This effect can be explained by longer frame duration. Consequently the tracking of the Doppler variation as well as the CFO is more difficult to perform at low level of SNR. It should be noticed that increasing the size of the preamble yields only marginal improvement.

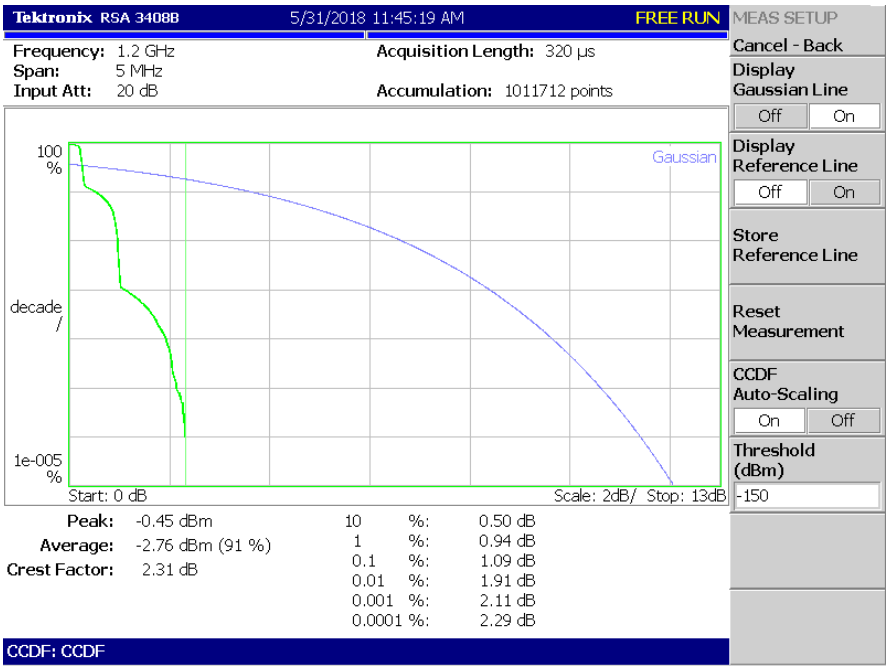

Figure 11: CDF of crest factor for TFSK waveform

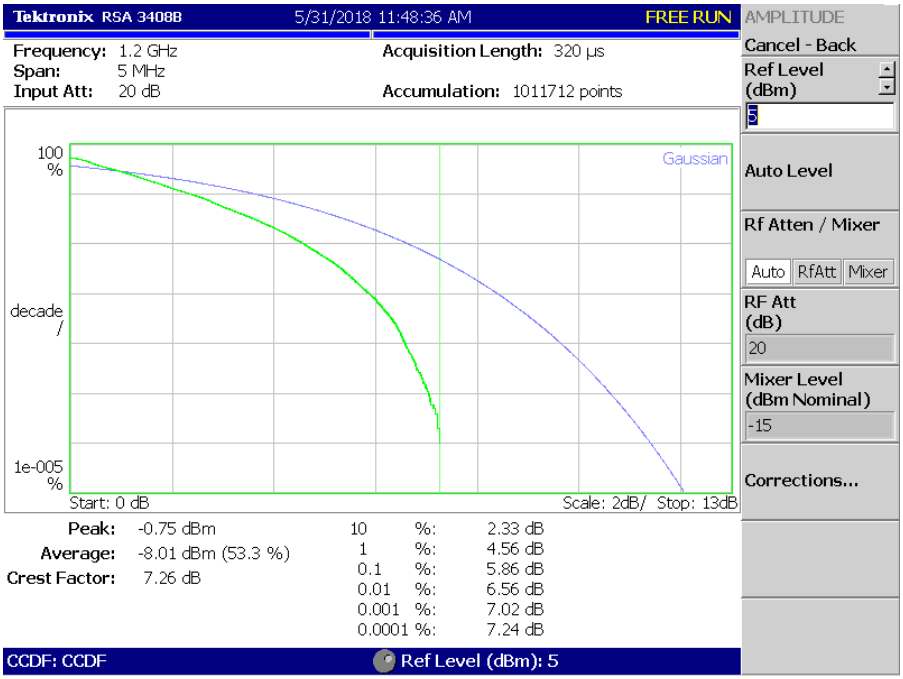

Figure 12: CDF of crest factor for NB IoT waveform

Figure 11 and Figure 12 show the crest factor CDF for both NB-IoT and turbo-FSK waveforms. As expected, turbo-FSK exhibits a much lower crest factor. Note that the theoretical crest factor in RF is 3dB larger than the baseband crest factor.

3 Positioning with combination of satellite and 5G

3.1 Test configuration

3.1.1 Test location and date

The testing phase has been performed at Thales Alenia Space premises. Tests in real conditions involved the use of:

-GNSS signals from real satellite constellations,

-streams of 5G data from a server simulating 5G observations.

3.1.2 Overall testing architecture

The figure below shows the overall architecture of the satellite/mm-wave positioning solution:

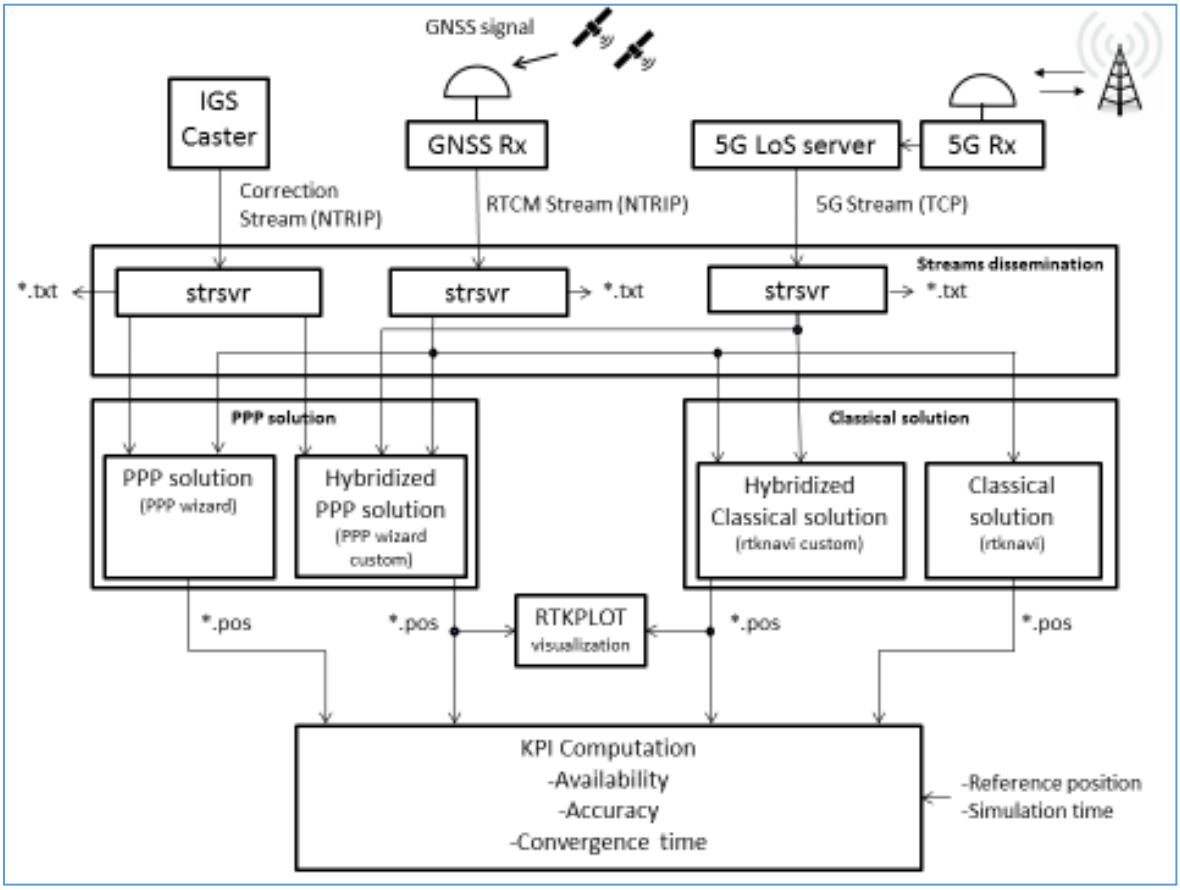

Figure 13 : Overall testing architecture

3.1.3 Hardware configuration

The main components of the hardware configuration are:

- TAS laptop for PPP computing
- TPZ laptop for standard positioning, stream dissemination and hosting the 5G LOS server.
- TAS GNSS receiver Ublox M8-T for streams collection
- Local network hosted by TPZ/TAS smartphone for stream exchange

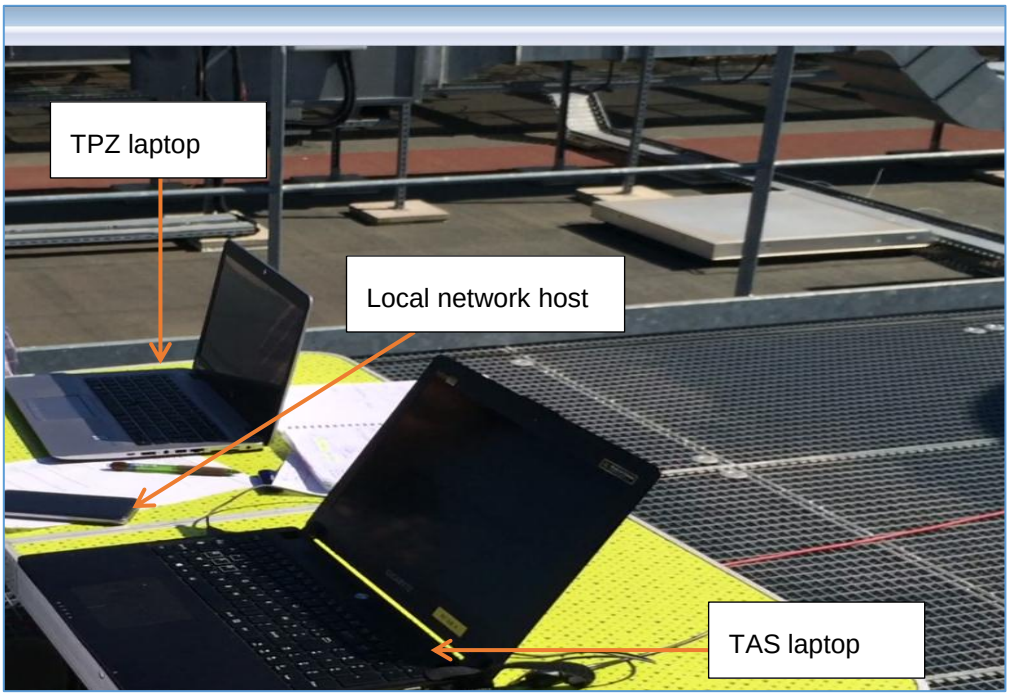

Figure 14: Hardware configuration

Figure 15: GNSS receiver

3.1.4 Software configuration

The following software are used in the testing phase:

- Oulu server for sending the 5G LOS measurement information (angular domain measurements) encapsulated in UDP IP packets. Each measurement is associated with the standard deviation error, which is derived from the error associated to beamwidth and step size of the neighbouring beams. Numerology used in this tests are following: azimuth beamwidth is 60 deg / 8 = 7.5 deg [D3.3], [EUCAP2018], and algorithm is running two level beam scanning. The result from the first level (coarse estimate) is divided to the smaller scan area (fine tuning); While the beam width is same (as number of active antenna elements is same), we reduce the step size between the beams for second level scanning. The final result is associated with the std error due to the fact that result lies anywhere within the beam step size. We model this uncertainty assuming the uniform random distribution, and thus the resulting std err is 0.8299 (2 level method) or 2.1651 (1 level method)..

- The RTKLIB executable “strsvr” for dissemination of streams

- The stock and modified RTKLIB executable “rtkrcv” for computation of the standard and hybridized solution as well as saving solution under *.pos format [RD0].

- Stock and modified PPP wizard software for computation of the standard and hybridized PPP solution as well as saving solution under *.pos format.

- The RTKLIB executable “rtkplot” for visualization of the solutions in real time during the test phase.

- A Matlab routine for KPI computation.
- Stock and modified PPP wizard software [ION2015] for computation of the standard and hybridized PPP solution as well as saving solution under *.pos format.

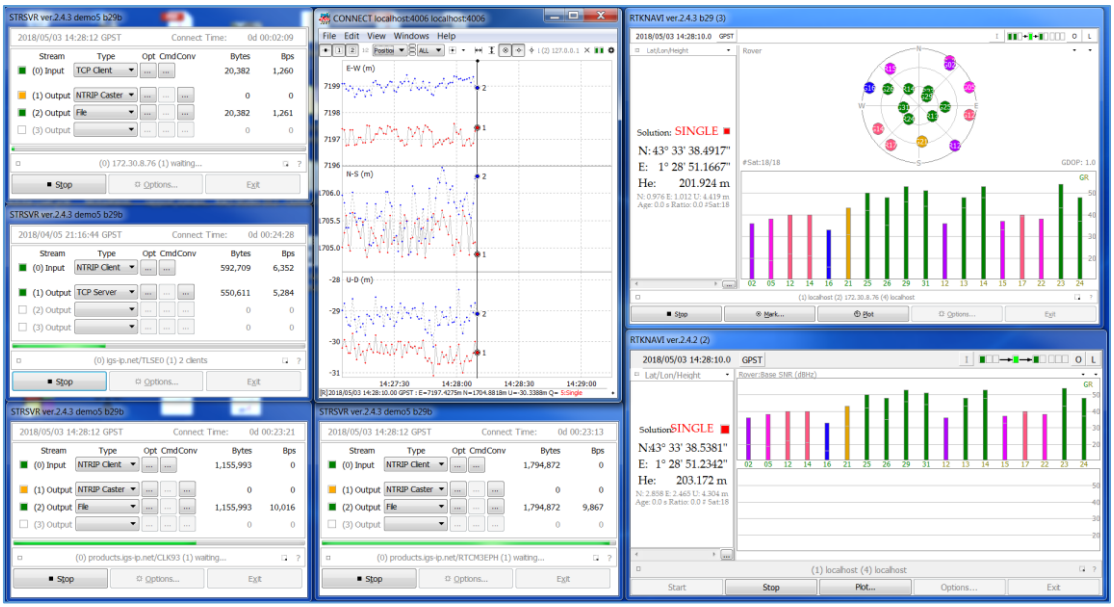

Figure 16: Software configuration

3.2 Test requirements

Prior to the definition of test cases, some requirements need to be defined such as the selection of the constellation or the visibility conditions.

3.2.1 GNSS requirements

[req_000]: Title: “GNSS constellation selection”.
When GNSS signals are involved, satellites from GPS, GALILEO and GLONASS constellations have to be taken into account (Dual Constellation).

[req_001]: Title: “GNSS Signal selection”.
When GNSS signals are involved, only the E1/L1 carrier frequency has to be used (Single frequency).

3.2.2 5G requirements

[req_010]: Title: “5G station selection”.
The least number of 5G station (mathematically) has to be taken into account.

- One 5G station for hybrid positioning solutions,
- Two 5G stations for the 5G standalone solution.

[req_011]: Title “5G station location”.
The exact location of the 5G station is provided by the 5G stream. Please refer to appendix for 5G stream information.

[req_011]: Title “5G station location accuracy”.
The accuracy of the location of the 5G station is high enough to not provide associated standard deviation. Please refer to appendix for 5G stream information.

[req_012]: Title “5G station observation”.
The observations form the 5G station (azimuth, elevation) are provided by the 5G stream. Please refer to appendix for 5G stream information.

[req_013]: Title “5G observation accuracy”.
The accuracy of the 5G observations is provided in the 5G stream under standard deviation information. Please refer to appendix for 5G stream information.

3.2.3 Visibility requirements

[req_020]: Title: “Clear Sky Environment”.
The record of observations is done on TAS roof top with no obstruction for satellite visibility and minimum amount of multipath. For the representativeness of a clear sky configuration an elevation mask of 10 degrees is applied on every satellite.

The true position of the GNSS receiver antenna in LLH coordinates is:

- Latitude = 43.54538233 deg
- Longitude = 1.39180051 deg
- Height = 227.98 m

[req_021]: Title: “Urban Environment”.
The record of observations is done on TAS campus at the foot of the buildings. The location has been chosen to provide an accurate representation of urban conditions.. For the

representativeness of an urban configuration an elevation mask of 10 degrees is applied on every satellite.

The true position of the GNSS receiver antenna in LLH coordinates is:

- Latitude = 43.54580336 deg
- Longitude = 1.39179602 deg
- Height = 189.07 m

[req_022]: Title: “Canyon Environment”.
Observations on canyon environment are the observations on urban environment plus 45 degrees of elevation mask. Moreover, in order to create extreme condition of visibility (less than 3 satellites) it has been chosen to use the GPS constellation only.

The true position of the receiver antenna is the position of the receiver antenna on urban environment.

[req_023]: Title: “Light Indoor Environment”.
The record of observations is done inside the TAS building near a window. No elevation mask is applied on visible satellites.

The true position of the GNSS receiver antenna in LLH coordinates is:

- Latitude = 43.54579604 deg
- Longitude = 1.39179261 deg
- Height = 189.07 m

[req_024]: Title: “5G visibility”.

The following positions of the 5G stations relative to the UE position are to be tested.

- N20: North 20 meters (azimuth angle equals 180 deg from the 5G station)
- N50: North 50 meters (azimuth angle equals 180 deg from the 5G station)
- N20 E20: North 20 meters and East 20 meters (2 5G stations: 180deg and 270deg)
- N50 E50: North 50 meters and East 50 meters (2 5G stations: 180deg and 270deg)
- N20 SE20: North 20 meters and South-East 20 meters (2 5G stations: 180deg and 315deg)

N50 SE50: North 50 meters and South-East 50 meters (2 5G stations: 180deg and 315deg)

Table 1: True position of the GNSS receiver antenna in LLH coordinates

Direction	North		East		South East	
Range [m]	20	50	20	50	20	50
Clear Sky [deg/deg/m]	43.54556234 1.39180051 227.98	43.54583235 1.39180051 227.98	43.54538233 1.39204798 227.98	43.54538233 1.39241918 227.98	43.54525505 1.39197549 227.98	43.54506412 1.39223797 227.98
Urban/Canyon [deg/deg/m]	43.54598336 1.39179602 189.07	NA	43.54580336 1.39204349 189.07	NA	43.54567607 1.39197101 189.07	NA
Light indoor [deg/deg/m]	43.54597605 1.39179261 189.07	NA	43.54579604 1.39204008 189.07	NA	43.54566876 1.39196760 189.07	NA

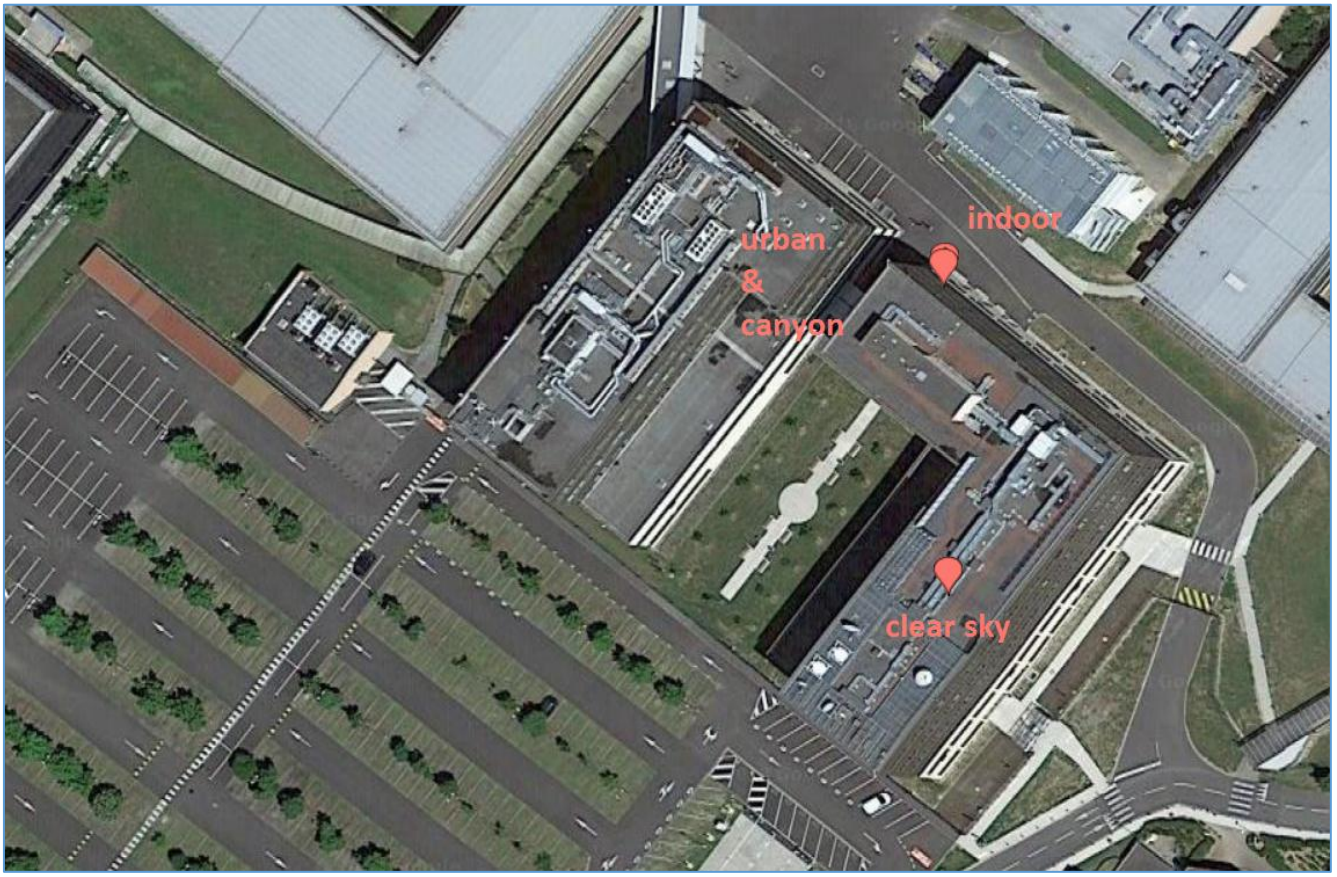

Figure 17: Test locations

3.3 Test plan

The test plan is divided into test cases following the environment sections. For each test case, all of the positioning solutions are assessed.

3.3.1 Test cases

[TC_001]: “Clear Sky Environment”.

The procedure has to be repeated for the following 5G visibility: N20, N50, N20 E20, N50 E50, N20 SE20 and N50 SE50.

- **Procedure:**
  - Test bed is run under clear sky environment.
  - GPS, GALILEO and GLONASS signals are used in the L1 band.
  - Instant of start and end of the simulation are recorded for KPI computation.
  - Input streams (5G stream, GNSS observation stream and correction stream) are recorded in separated files for post processing purpose.
  - Output streams (PPP streams and standard solution stream) are recorded in separated files for post processing purpose.
- **Compliance criteria:**
  The good record of each stream and start/stop instants provides the success criteria.

[TC_002]: “Urban Environment”.

The procedure has to be repeated for the following 5G visibility: N20, N20 E20 and N20 SE20.

- **Procedure:**
  - Test bed is run under urban environment.
  - GPS, GALILEO and GLONASS signals are used in the L1 band.
  - Instant of start and end of the simulation are recorded for KPI computation.
  - Input streams (5G stream, GNSS observation stream and correction stream) are recorded in separated files for post processing purpose.
  - Output streams (PPP streams and standard solution stream) are recorded in separated files for post processing purpose.
- **Compliance criteria:**
  The good record of each stream and start/stop instants provides the success criteria.

[TC_003]: “Canyon Environment”.

The procedure has to be repeated for the following 5G visibility: N20, N20 E20 and N20 SE20.

- **Procedure:**
  - Test bed is run under canyon environment.
  - GPS signals are used in the L1 band.
  - Instant of start and end of the simulation are recorded for KPI computation.
  - Input streams (5G stream, GNSS observation stream and correction stream) are recorded in separated files for post processing purpose.

- Output streams (PPP streams and standard solution stream) are recorded in separated files for post processing purpose.

- **Compliance criteria:**
  The good record of each stream and start/stop instants provides the success criteria.

[TC_004]: “Light Indoor Environment”.

The procedure has to be repeated for the following 5G visibility: N20, N20 E20 and N20 SE20.

- **Procedure:**
  - Test bed is run under light indoor environment.
  - GPS, GALILEO and GLONASS signals are used in the L1 band.
  - Instant of start and end of the simulation are recorded for KPI computation.
  - Input streams (5G stream, GNSS observation stream and correction stream) are recorded in separated files for post processing purpose.
  - Output streams (PPP streams and standard solution stream) are recorded in separated files for post processing purpose.
- **Compliance criteria:**
  The good record of each stream and start/stop instants provides the success criteria.

3.3.2 Test proceedings

The data collection and demonstrations are done accordingly to the test plan, with an Ublox receiver at Thales Alenia Space premises (figure 5). Receivers positions are presented below for the three environments:

Figure 18: View of test site

Figure 19 : View of test site (Urban environment)

Figure 20: View of test site (Light indoor environment)

3.4 Test report

3.4.1 Approach

The comparison of each positioning solution has to be compared on the same KPIs.

The following KPI are computed from test records:

- Availability of the solution is the percentage of time the solution is available considering 1Hz for the delivering rate of the solution.
- Accuracy of the solution:
  - Mean horizontal error,
  - Standard deviation of the horizontal error,
  - 70th, 95th and 99th percentile of the horizontal error.
- Convergence time of the solution is the amount of time required to stay below one meter of horizontal positioning error.

3.4.2 Results

3.4.2.1 Clear Sky

The clear sky record starts at: 05/04/2018 13:12:54 or GPST: 1206969174

The measurement lasts exactly 1h00m00s.

3.4.2.1.1 N20

The user is placed at 20 m from two 5G BS placed at South-East and North.

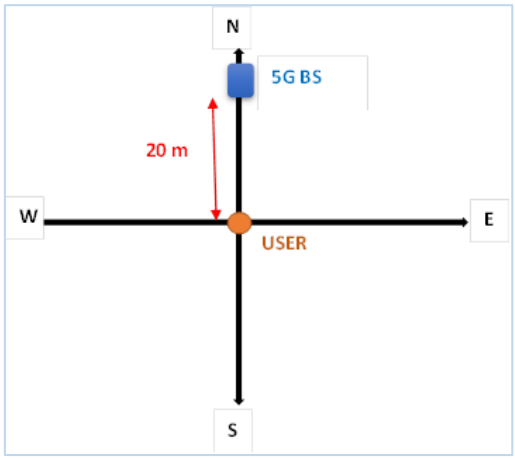

Figure 21: N20 case

3.4.2.1.1.1 Plot

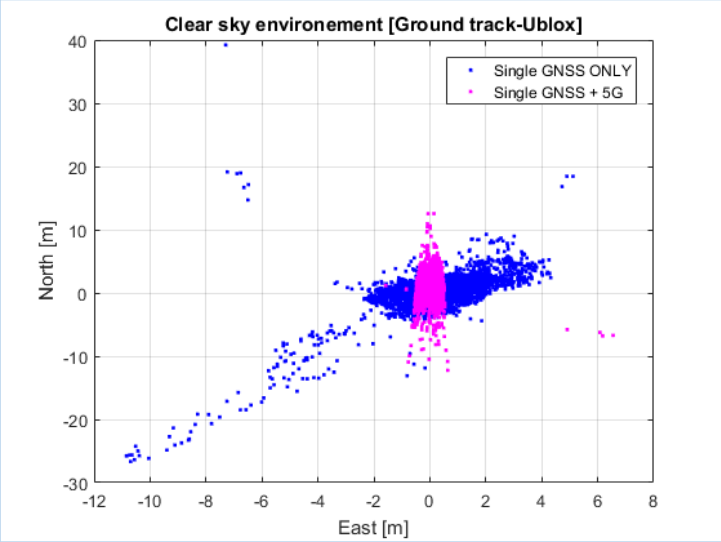

Figure 22: Ground track (Single positioning)

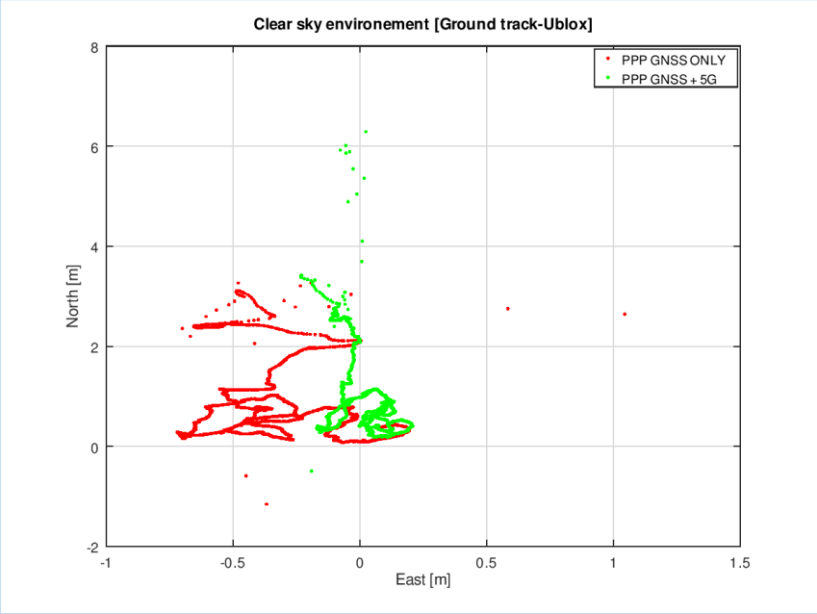

Figure 23: Ground track (PPP) Clear sky N20

The spreading of the hybridized position is contained within the external line of sight from the 5G base station. As the base station is at the north from the receiver, the east-west accuracy is improved with respect to the single positioning and precise positioning. Nevertheless the north-south accuracy stay unchanged.

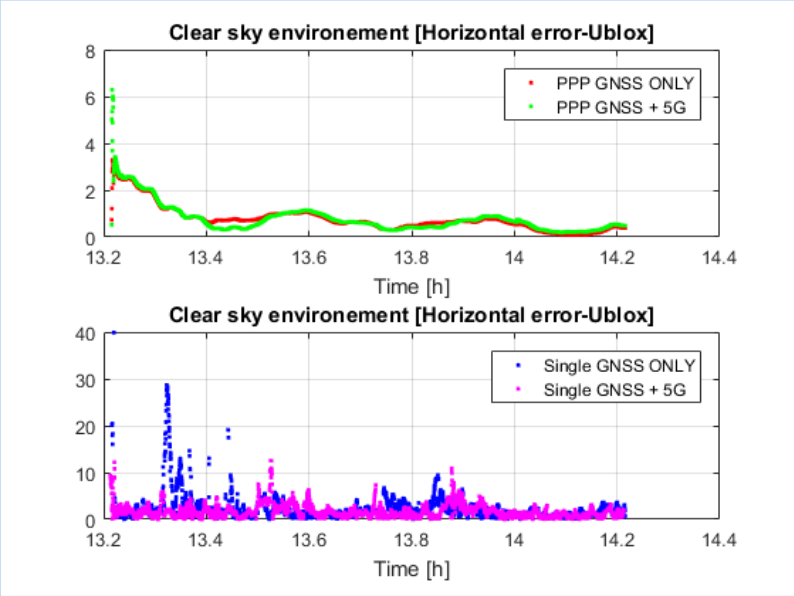

Figure 24: Horizontal errors (Clear sky N20)

The order of magnitude of the horizontal accuracy of the single-hybridized solution is the same as the single positioning due to the lack of improvement in the north-south direction.

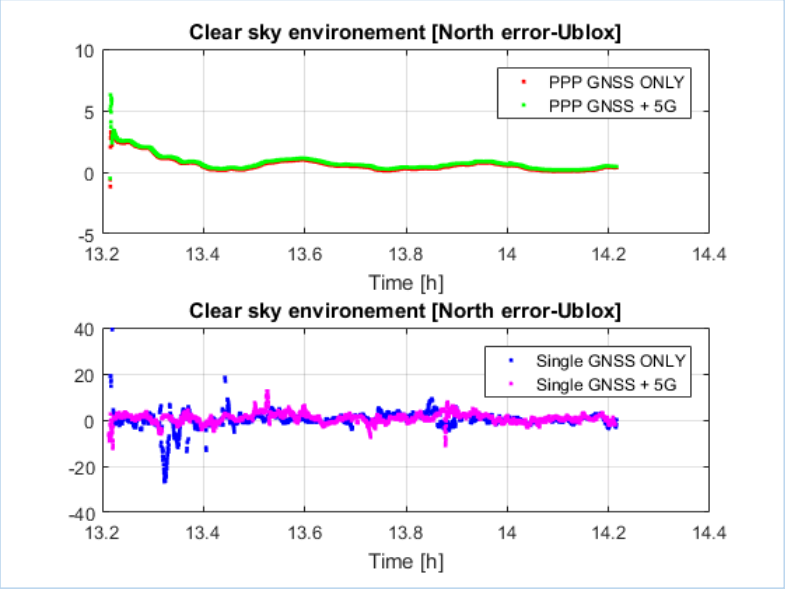

Figure 25: North errors (Clear sky N20)

As previously foreseen on the spreading of the solutions, the accuracy in the north-south direction is not improved due to the use of a single base station in the north direction.

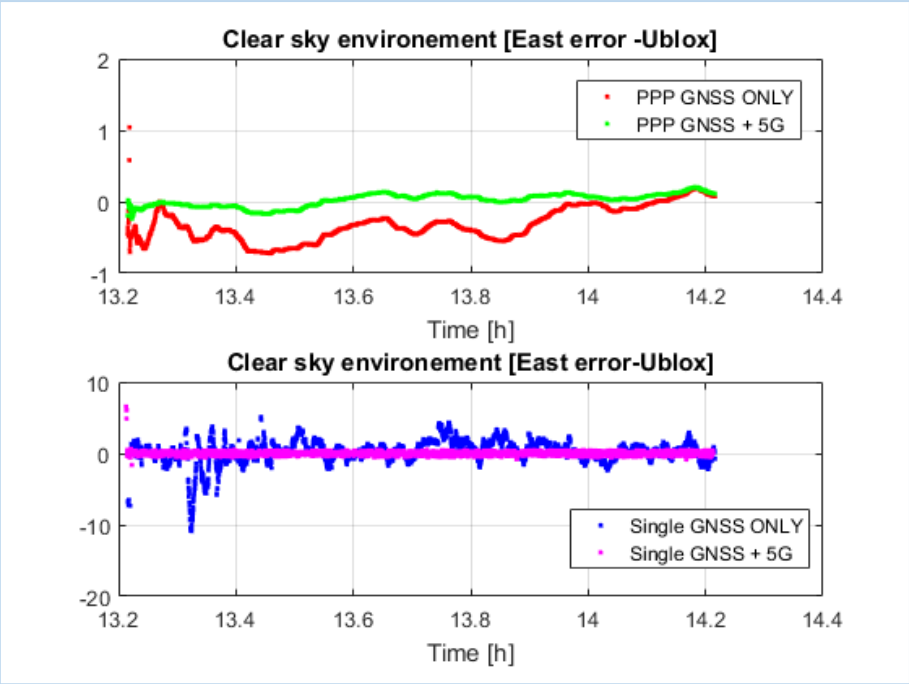

Figure 26: East errors (Clear sky N20)

As previously foreseen on the spreading of the solutions, the accuracy in the east-west direction is improved thanks to the use of a base station in the north direction.

3.4.2.1.1.2 KPI

Table 2 :KPI (clear sky N20)

Method	Availability [%]	Accuracy [m]					Convergence time [min]
		Mean	Std	70th prctl	95th prctl	99th prctl	
PPP	99.917	0.4918	0.2236	0.6342	0.7905	0.9643	23.53
PPP +5G	99.999	0.5198	0.2103	0.6474	0.8899	0.9591	24.30
Single	98.890	1.8450	1.2786	2.1469	4.2441	6.4483	NA
Single +5G	99.805	1.4550	1.1926	1.7086	3.9087	5.8123	NA

3.4.2.1.2 N50

The user is placed at 50 m from two 5G BS placed at South-East and North.

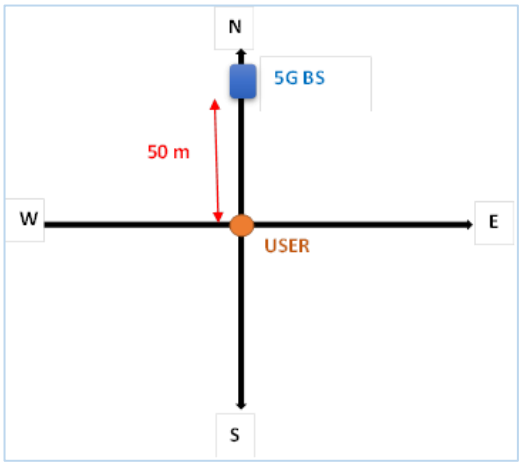

Figure 27: N50 case

3.4.2.1.2.1 Plot

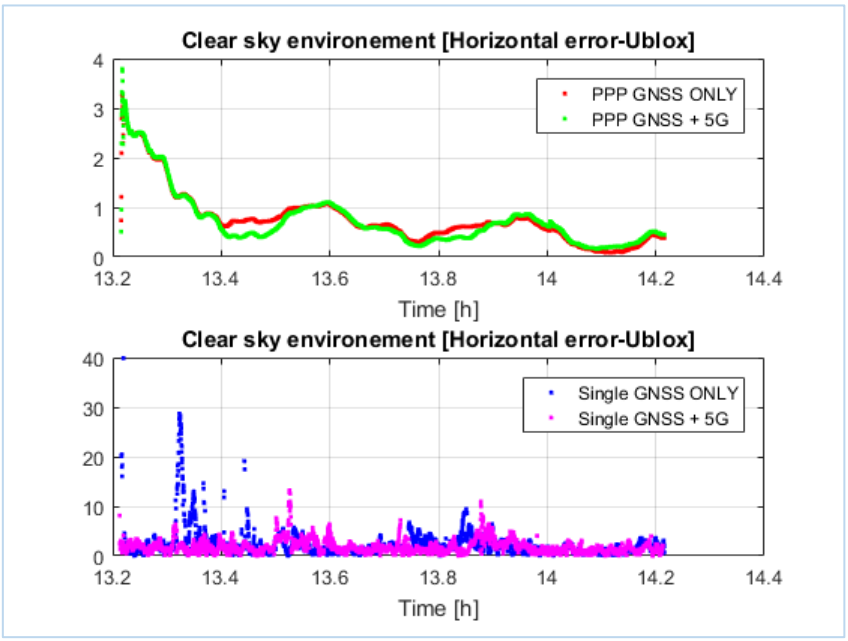

Figure 28: Horizontal errors (clear sky N50)

Same observations as the N20 test case can be done. The overall spreading of the hybridized solution, compared to the classical spreading, is contained within the external line of sight from the 5G base stationflattened on the 5G LOS. As the base station if further away

from the receiver (compared to 20 meters), the east-west spreading is wider for the hybridized solution. The north-south error is not reduced by the 5G observation since the direction of the error is aligned with the line of sight (5G BS located on the north).

3.4.2.1.2.2 KPI

Table 3 : KPI (clear sky N50)

Method	Availability [%]	Accuracy [m]					Convergence time [min]
		Mean	Std	70th prctl	95th prctl	99th prctl	
PPP	99.917	0.4918	0.2236	0.6342	0.7905	0.9643	23.53
PPP +5G	99.917	0.4835	0.2134	0.6020	0.8596	0.9623	23.86
Single	98.890	1.8450	1.2786	2.1469	4.2441	6.4483	NA
Single +5G	100.000	1.6350	1.1663	1.8726	4.0627	5.7538	NA

3.4.2.1.3 N20 E20

The user is placed at 20 m from two 5G BS placed at East and North.

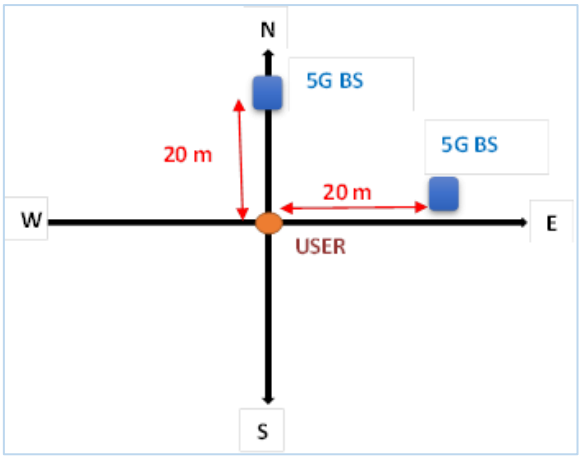

Figure 29: N20 E20 case

3.4.2.1.3.1 Plot

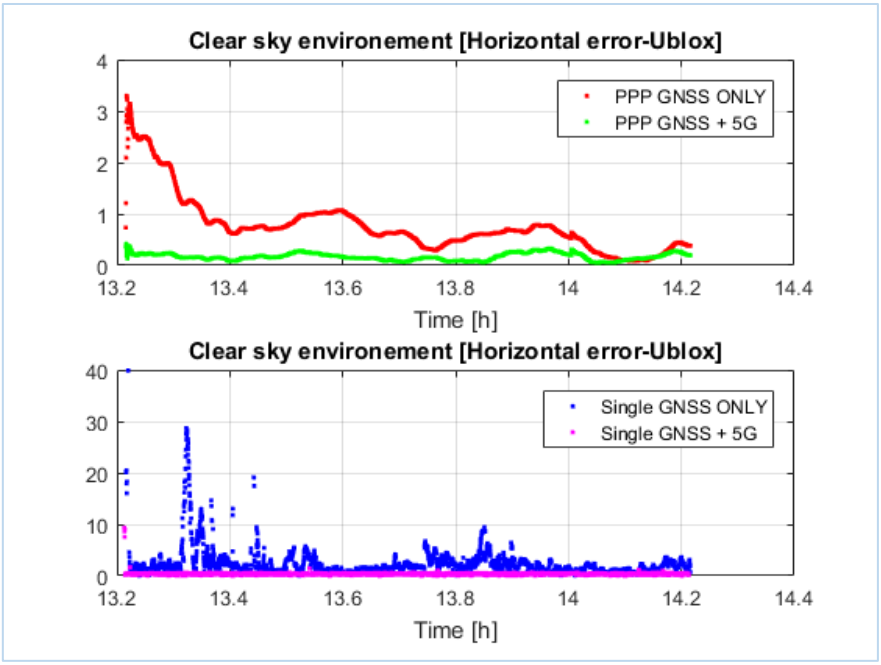

Figure 30: Horizontal errors (clear sky N20 E20)

As foreseen with the spreading plot, the horizontal accuracy is reduced thanks to the use of 2 base stations.

3.4.2.1.3.2 KPI

Table 4 : KPI (clear sky N20E20)

Method	Availability [%]	Accuracy [m]					Convergence time [min]
		Mean	Std	70th prctl	95th prctl	99th prctl	
PPP	99.917	0.4918	0.2236	0.6342	0.7905	0.9643	23.53
PPP +5G	99.917	0.1724	0.06799	0.2157	0.2867	0.3201	0
Single	98.890	1.8450	1.2786	2.1469	4.2441	6.4483	NA
Single +5G	99.750	0.3815	0.1500	0.4675	0.5955	0.6627	NA

3.4.2.1.4 N50 E50

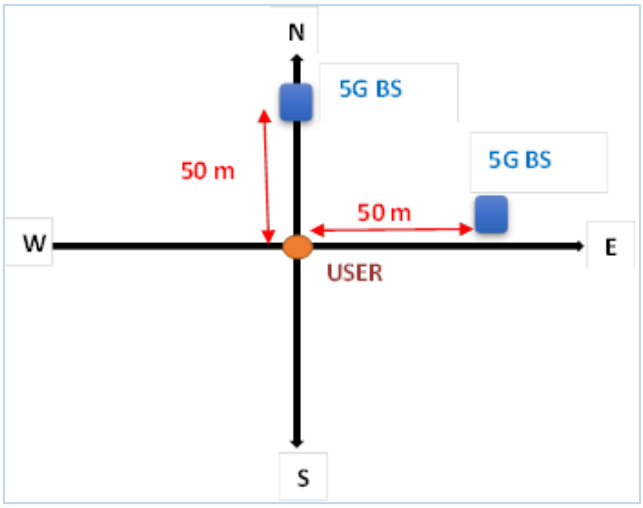

Figure 31: N50 E50 case

3.4.2.1.4.1 Plot

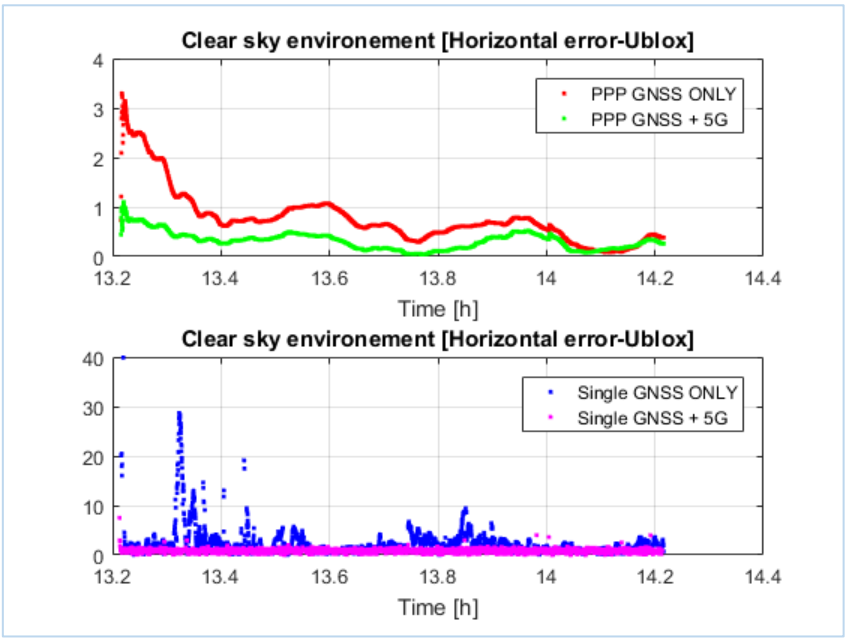

Figure 32: Horizontal errors(clear sky N50 E50)

3.4.2.1.4.2 KPI

Table 5 : KPI (clear sky N50E50)

Method	Availability [%]	Accuracy [m]					Convergence time [min]
		Mean	Std	70th prctl	95th prctl	99th prctl	
PPP	99.917	0.4918	0.2236	0.6342	0.7905	0.9643	23.53
PPP +5G	99.917	0.3160	0.1710	0.4012	0.6342	0.7517	0.36
Single	98.890	1.8450	1.2786	2.1469	4.2441	6.4483	NA
Single +5G	99.944	0.8936	0.3793	1.0923	1.4368	1.6883	NA

3.4.2.1.5 N20 SE20

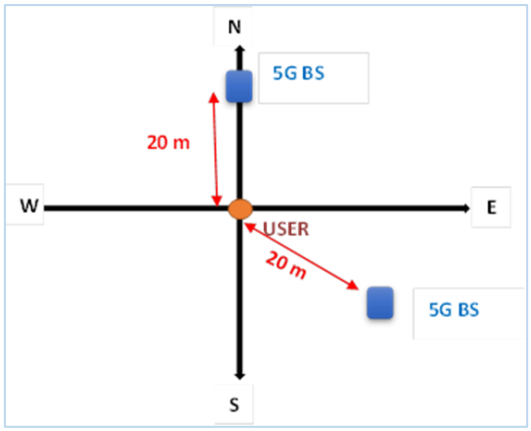

Figure 33: Clear sky N20 SE20 case

3.4.2.1.5.1 Plot

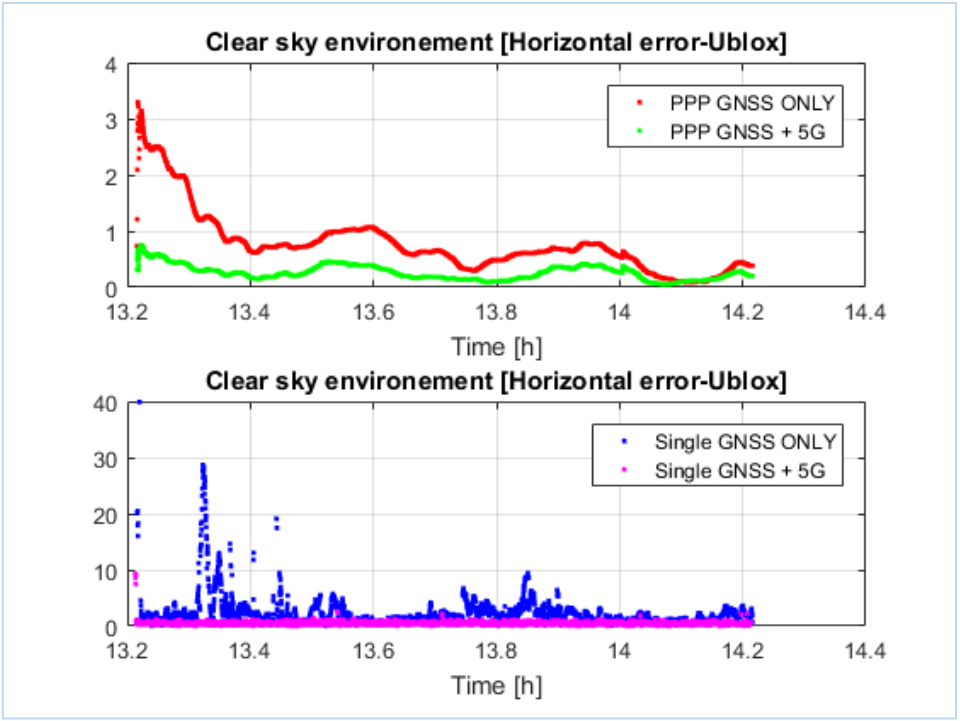

Figure 34: Horizontal errors (clear sky N20 SE20)

3.4.2.1.5.2 KPI

Table 6: KPI (clear sky N20SE20)

Method	Availability [%]	Accuracy [m]					Convergence time [min]
		Mean	Std	70th prctl	95th prctl	99th prctl	
PPP	99.917	0.4918	0.2236	0.6342	0.7905	0.9643	23.53
PPP +5G	99.917	0.2651	0.1311	0.3310	0.4664	0.6228	0
Single	98.890	1.8450	1.2786	2.1469	4.2441	6.4483	NA
Single +5G	99.722	0.5179	0.2729	0.6220	1.0078	1.1598	NA

3.4.2.1.6 N50 SE50

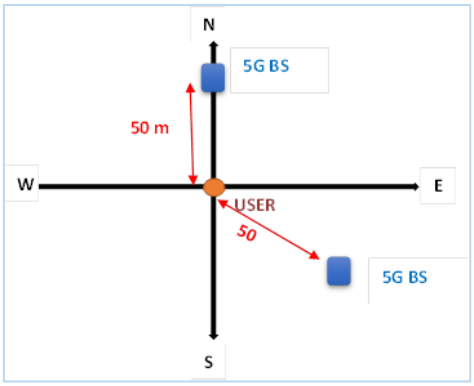

Figure 35: Clear sky N50 SE50 case

3.4.2.1.6.1 Plot

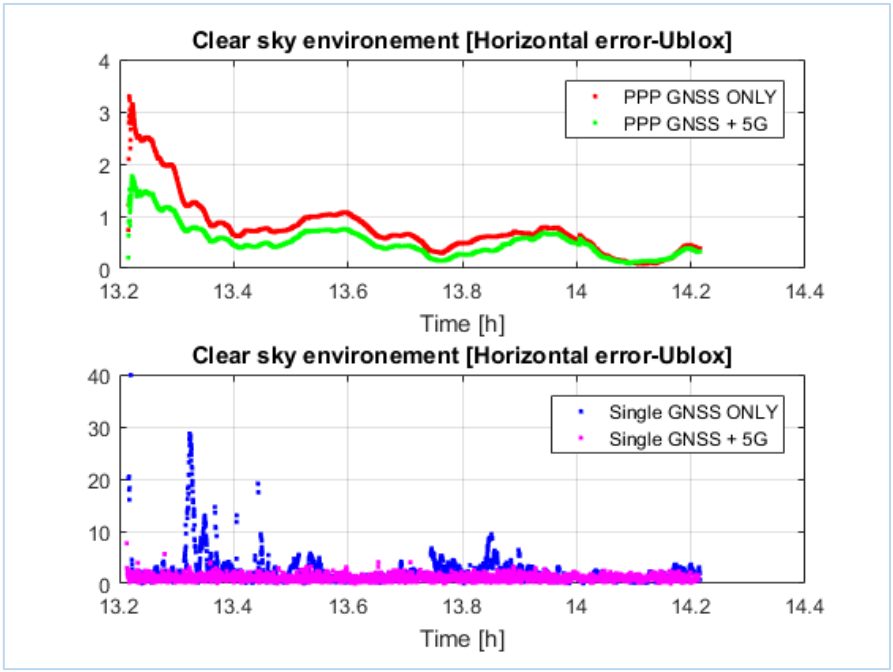

Figure 36: Horizontal errors(clear sky N50 SE50)

3.4.2.1.6.2 KPI

Table 7: KPI (clear sky N50SE50)

Method	Availability [%]	Accuracy [m]					Convergence time [min]
		Mean	Std	70th prctl	95th prctl	99th prctl	
PPP	99.917	0.4918	0.2236	0.6342	0.7905	0.9643	23.53
PPP +5G	99.917	0.4474	0.1950	0.5637	0.7437	0.8006	5.116
Single	98.890	1.8450	1.2786	2.1469	4.2441	6.4483	NA
Single +5G	99.861	1.0974	0.5661	1.2787	2.1823	2.7242	NA

3.4.2.1.7 Conclusion on clear sky results

Sub-metric accuracy is reached by the PPP method even without the help of 5G stations, due to the very good satellite visibility and strong signal power received in the clear sky environment.

Without PPP (single method), sub-metric accuracy can be reached with the help of two 5G antennas at less than 50m from the user.

3.4.2.2 Urban

The urban record starts at: 08/03/2018 16:43:40 or GPST: 1204562620

The measurement lasts exactly 1h00m00s.

During the computing phase of both the single solution and single + 5G solution, a power mask of 40dB has been applied on the observations. Without this power mask the availability dropped down to few percent. No power mask has been applied in PPP case.

3.4.2.2.1 N20

3.4.2.2.1.1 Plot

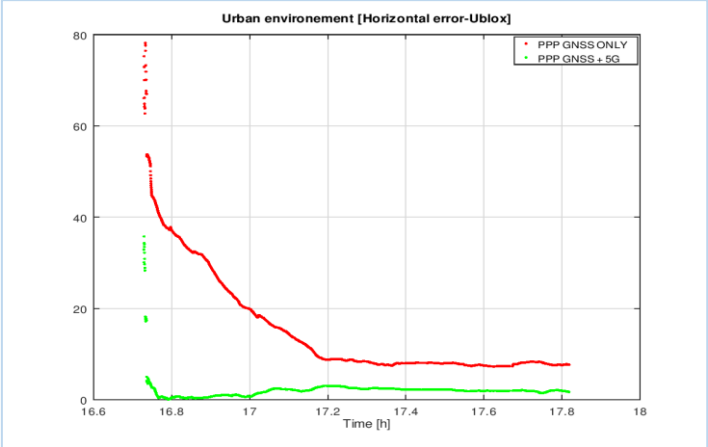

Figure 37: Horizontal errors (PPP Urban N20)

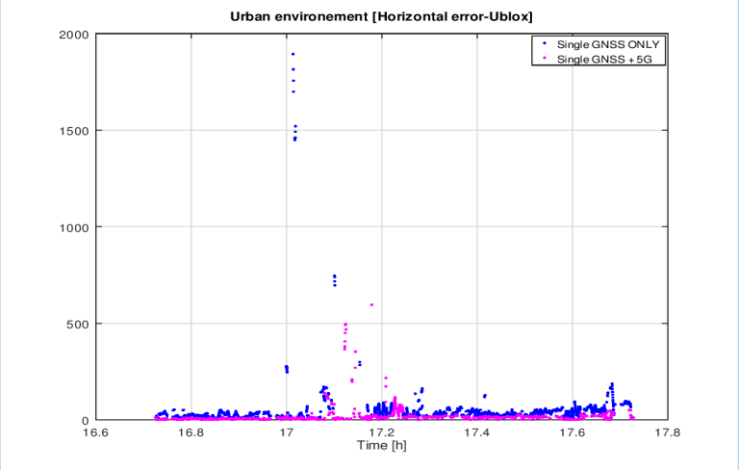

Figure 38: Horizontal errors (Single positioning Urban N20)

3.4.2.2.1.2

3.4.2.2.1.3 KPI

Table 8: KPI (Urban N20)

Method	Availability [%]	Accuracy [m]					Convergence time [min]
		Mean	Std	70th prctl	95th prctl	99th prctl	
PPP	91.722	15.1743	11.5088	16.0685	37.9747	53.1703	No convergence
PPP +5G	91.722	2.0121	2.0703	2.2698	3.0023	4.0230	No convergence
Single	72.125	41.7893	101.7684	40.3888	84.8259	175.0588	NA
Single +5G	77.645	14.5040	30.0055	14.8720	31.6625	114.1913	NA

The horizontal accuracy presents an improvement with 5G observations. In general the accuracy measures considered show that with one 5G BS the horizontal positioning error can be reduced in single or precise positioning. The quality of the measurements has more impact on GNSS only positioning leading to the increasing of the errors in Single positioning and the convergence time in precise positioning. The contribution of 5G can be clearly observed in the hybridization results.

3.4.2.2.2 N20 E20

3.4.2.2.2.1 Plot

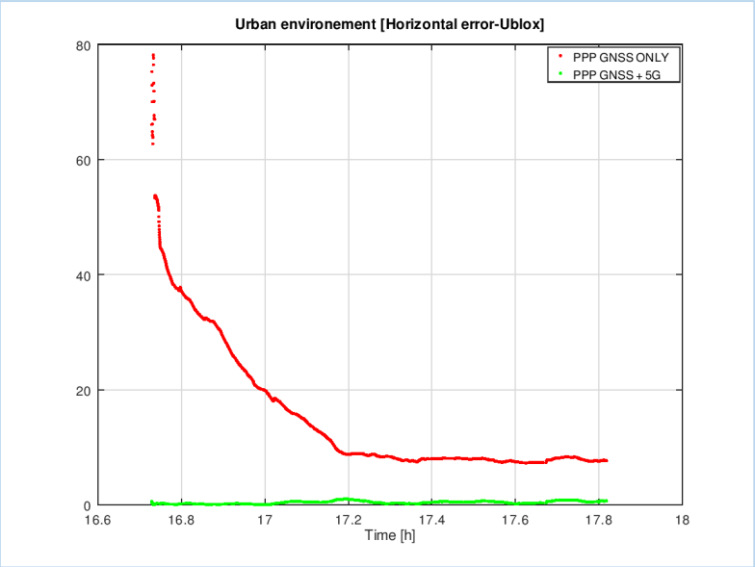

Figure 39: Horizontal errors (PPP Urban N20E20)

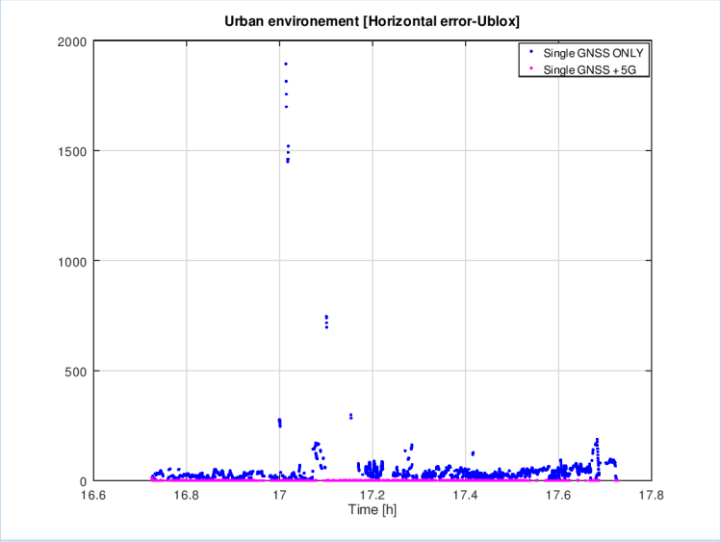

Figure 40: Horizontal errors (Single positioning Urban N20E20)

3.4.2.2.2.2 KPI

Table 9: KPI (Urban, N20E20)

Method	Availability [%]	Accuracy [m]					Convergence time [min]
		Mean	Std	70th prctl	95th prctl	99th prctl	
PPP	91.722	15.1743	11.5088	16.0685	37.9747	53.1703	No convergence
PPP +5G	91.722	0.4920	0.2018	0.5969	0.8362	0.9229	28.217
Single	72.125	41.7893	101.7684	40.3888	84.8259	175.0588	NA
Single +5G	72.396	0.4300	0.1985	0.5162	0.7447	0.9178	NA

3.4.2.2.3 N20 SE20

3.4.2.2.3.1 Plot

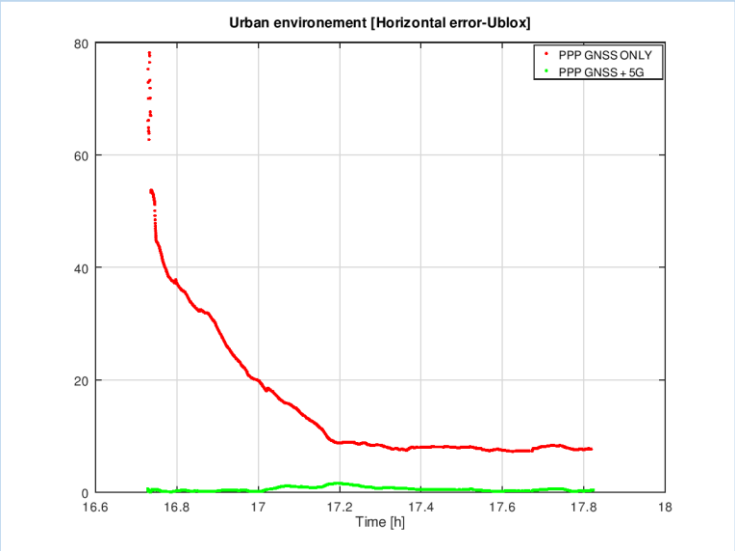

Figure 41: Horizontal errors (PPP Urban N20SE20)

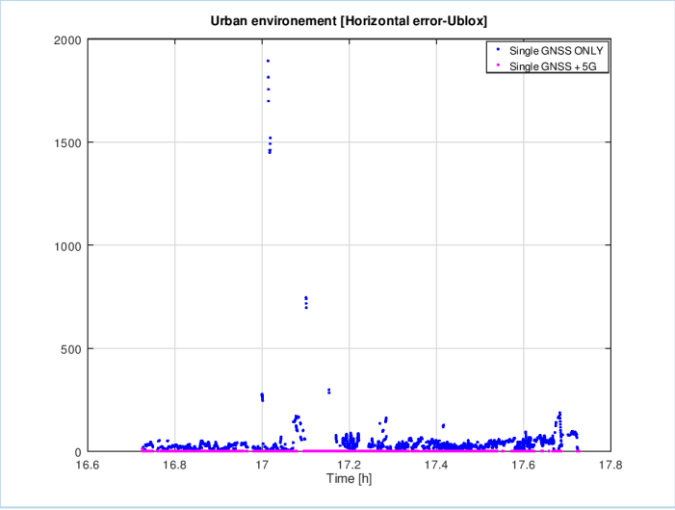

Figure 42: Horizontal errors (Single positioning Urban N20SE20)

3.4.2.2.3.2 KPI

Table 10: KPI (Urban N20SE20)

Method	Availability [%]	Accuracy [m]					Convergence time [min]
		Mean	Std	70th prctl	95th prctl	99th prctl	
PPP	91.722	15.1743	11.5088	16.0685	37.9747	53.1703	No convergence
PPP +5G	91.764	0.4786	0.2084	0.5724	0.8577	0.9490	31.833
Single	72.125	41.7893	101.7684	40.3888	84.8259	175.0588	NA
Single +5G	72.757	0.7250	0.4483	0.9038	1.6080	1.9006	NA

3.4.2.2.4 Conclusion on urban results

The addition of one 5G antenna to a GNSS system drastically improves the positioning accuracy in urban environments. The use of two antennas 20m away from the user can even lead to sub-metric errors.

3.4.2.3 Canyon

The canyon record starts at: 08/03/2018 16:43:40 or GPST: 1204562620

The measurement lasts exactly 1h00m00s.

The canyon environment is representative of an urban skyscraper environment: with a high elevation mask angle of 45° and few visible satellites (GPS only in the case below). Such kind of masking represents extremely sever visibility environment with less than 4 satellite in visibility during the whole record. During the first half hour only 2 satellite are visible and during the second half hour 3 satellites are visible. That is why computation of a fix in single or precise positioning with GNSS only is not successful : the assistance of another system (5G, wifi..) is required.

No power mask has been applied during the processing of the positions.

3.4.2.3.1 N20

3.4.2.3.1.1 Plot

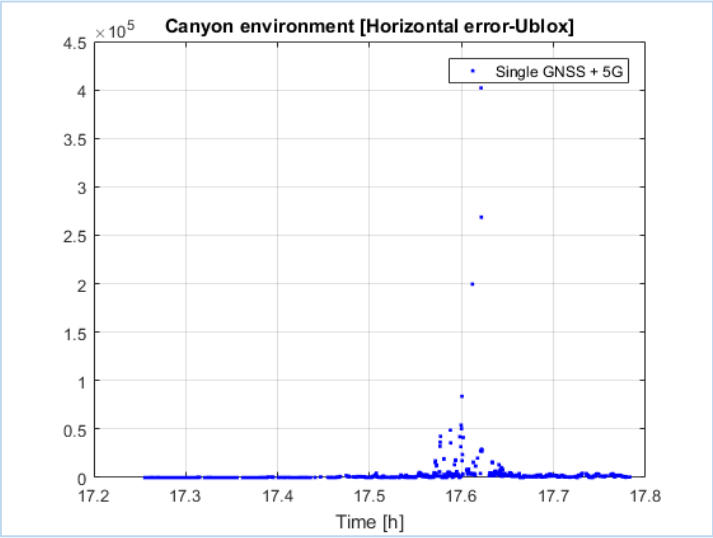

Figure 43: Horizontal errors (Single positioning Canyon N20)

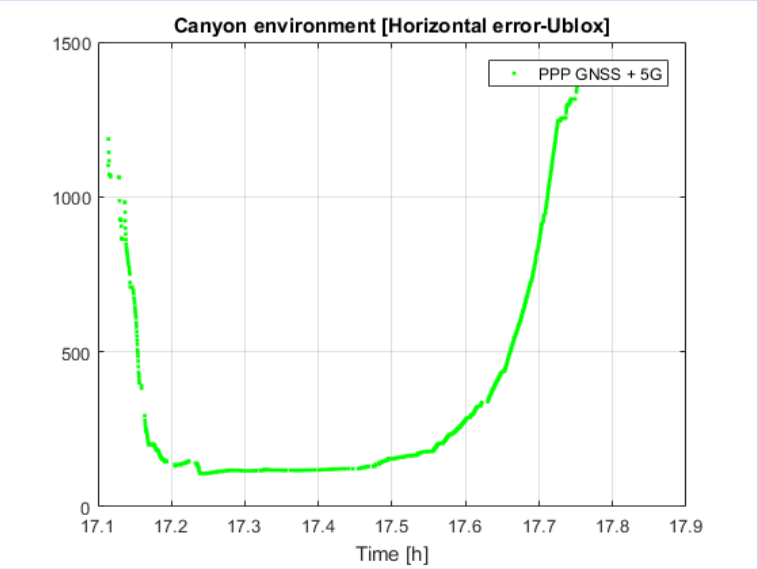

Figure 44: Horizontal errors (PPP Canyon N20)

The quality of the measurements impacts greatly on the performance of the precise positioning. As it can be seen, the solution is greatly degraded around the instant 17.6 ; this leads to the divergence of the filter in PPP case. This performance degradation can be observed in all the results presented in this section.

3.4.2.3.1.2 KPI

Table 11: KPI (Canyon N20)

Method	Availability [%]	Accuracy [m]					Convergence time [min]
		Mean	Std	70th prctl	95th prctl	99th prctl	
PPP	0	No fix	No fix	No fix	No fix	No fix	NA
PPP +5G	49.669	405.91	428.39	397.17	1402.5	1421.5	NA
Single	0	No fix	No fix	No fix	No fix	No fix	NA
Single +5G	39.458	2256.062	14277.0	1310.5	4880.8	28832.35	NA

The visibility of 3 satellites allows the hybridized processing to compute a fix with one 5G base station. As each base station is equivalent to 1 satellite (1 observation), the hybridized processing is not able to provide a solution with 2 satellites and 1 base station.

Even if the observation's accuracy of each base station is good at 20 meter away from the receiver (around tan(2.875*pi/180)*20=1m) the resulting global accuracy is degraded due to the fix spreading over the north-south direction (bad north-south accuracy). This fix spreading degrades more the PPP solution leading to a difficult convergence of the filter.

3.4.2.3.2 N20 E20

3.4.2.3.2.1 Plot

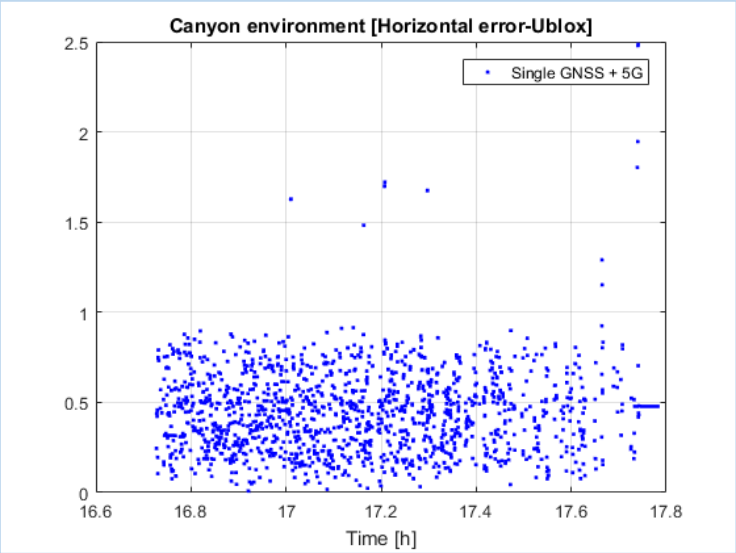

Figure 45: Horizontal errors (Single positioning Canyon N20E20)

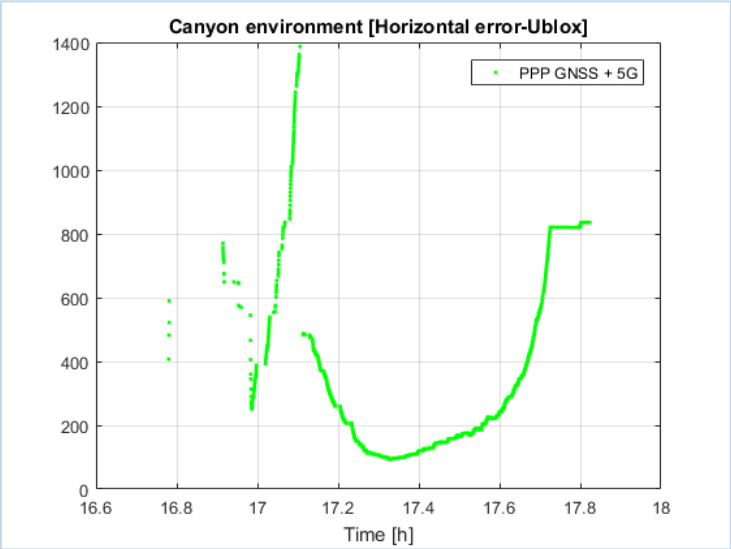

Figure 46: Horizontal errors (PPP Canyon N20E20)

3.4.2.3.2.2 KPI

Table 12: KPI (Canyon N20E20)

Method	Availability [%]	Accuracy [m]					Convergence time [min]
		Mean	Std	70th prctl	95th prctl	99th prctl	
PPP	0	No fix	No fix	No fix	No fix	No fix	NA
PPP +5G	61.556	341.22	277.27	384.71	835.27	1277.5	61.556
Single	0	No fix	No fix	No fix	No fix	No fix	NA
Single +5G	66.105	0.4006	0.1848	0.4787	0.6449	0.7272	NA

With 2 observations from 2 base stations the single and precise positioning is able to provide a good availability (over 61%) with at least 2 visible satellites. Though it is able to provide a solution PPP is not able to converge to a precise solution because of the great measurements diversity between epochs.

The use of 2 base stations with perpendicular line of sight (LOS) allows an optimized spreading of the fix and a minimum global error (under 1 meter for 99 percent of the fix).

3.4.2.3.3 N20 SE20

3.4.2.3.3.1 Plot

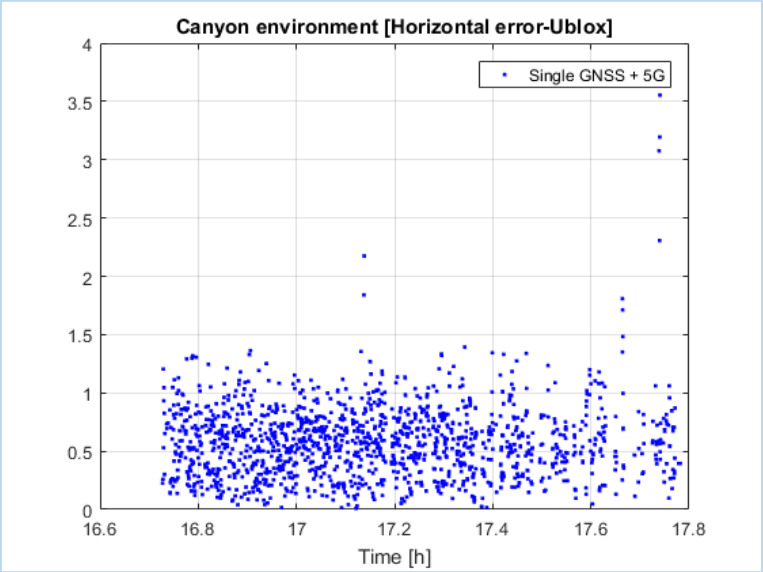

Figure 47: Horizontal errors (Single positioning Canyon N20SE20)

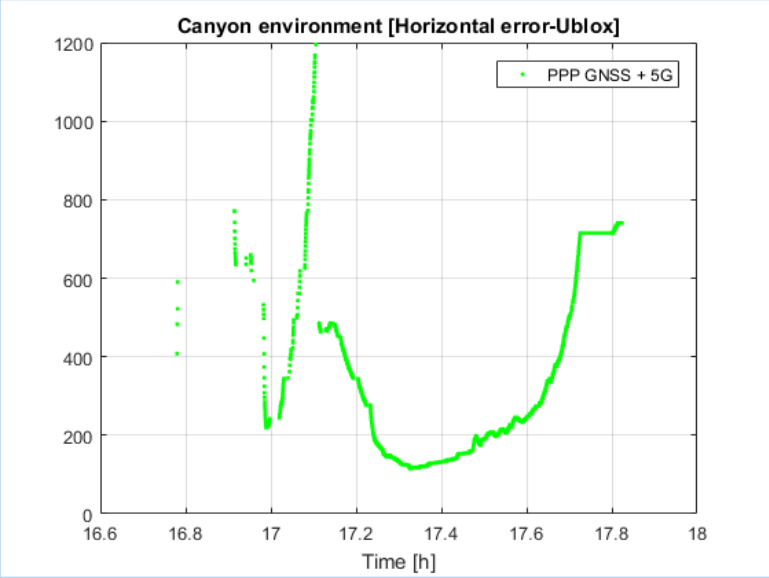

Figure 48: Horizontal errors (PPP Canyon N20SE20)

3.4.2.3.3.2 KPI

Table 13: KPI (Canyon N20SE20)

Method	Availability [%]	Accuracy [m]					Convergence time [min]
		Mean	Std	70th prctl	95th prctl	99th prctl	
PPP	0	No fix	No fix	No fix	No fix	No fix	NA
PPP +5G	61.556	328.55	220.86	386.21	715.44	1020.60	NA
Single	0	No fix	No fix	No fix	No fix	No fix	NA
Single +5G	66.157	0.51663	0.2800	0.6051	1.0286	1.1974	NA

3.4.2.3.4 Conclusion on canyon results

In canyon environments where GNSS positioning is very difficult or impossible, the addition of 5G stations is clearly valuable. However, the PPP algorithm has to be adapted in this kind of environment to be effectively useful.

3.4.2.4 Light Indoor

The urban record starts at: 09/03/2018 11:24:49 or GPST: 1204629889

The measurement lasts exactly 1h00m00s.

No elevation or power mask is applied during the light indoor processing. GPS, GLONASS and GALILEO constellations are used.

Every available observation is used to compute a solution. Indoor environment involves the use of low signal to noise ratio and leads to less accurate observations. That is why the global accuracy of the single processing is poor (>1000 for the 99th percentile).

3.4.2.4.1 N20

3.4.2.4.1.1 Plot

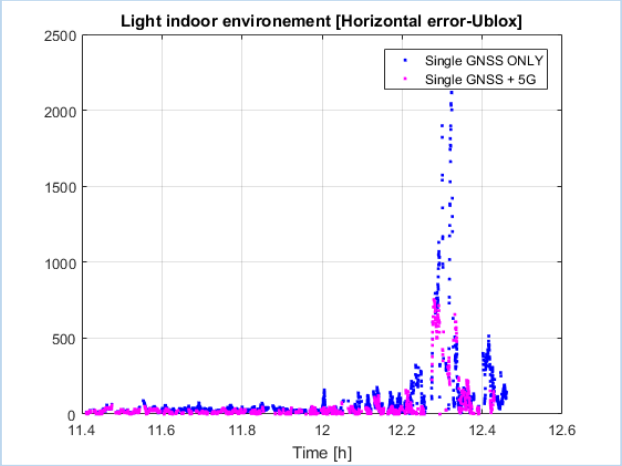

Figure 49: Horizontal errors (Single positioning Light Indoor N20)

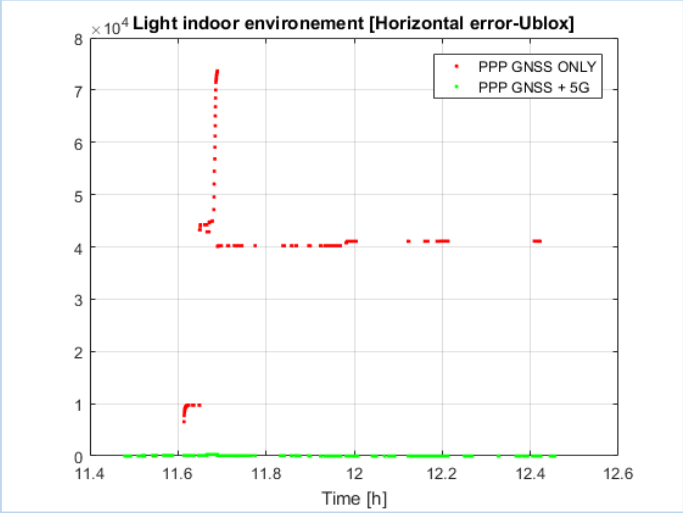

Figure 50: Horizontal errors (PPP Light Indoor N20)

3.4.2.4.1.2 KPI

Table 14: KPI (indoor N20)

Method	Availability [%]	Accuracy [m]					Convergence time [min]
		Mean	Std	70th prctl	95th prctl	99th prctl	
PPP	16.547	36060	15213	41080	44655	72892	NA
PPP +5G	33.706	58.91	77.87	75.89	304.5	304.7	NA
Single	71.671	81.34	206.60	43.73	317	1171	NA
Single +5G	51.380	49.93	116.59	30.22	212.4	637.5	NA

3.4.2.4.2 N20 E20

3.4.2.4.2.1 Plot

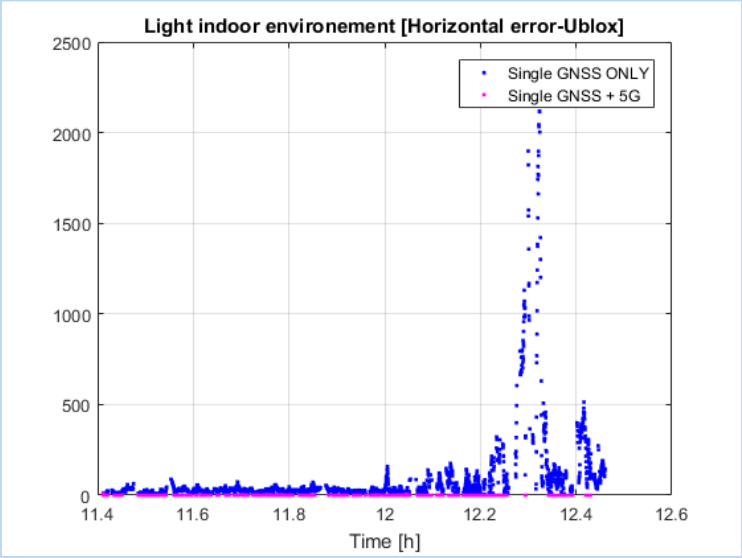

Figure 51: Horizontal errors (Single positioning Light Indoor N20E20)

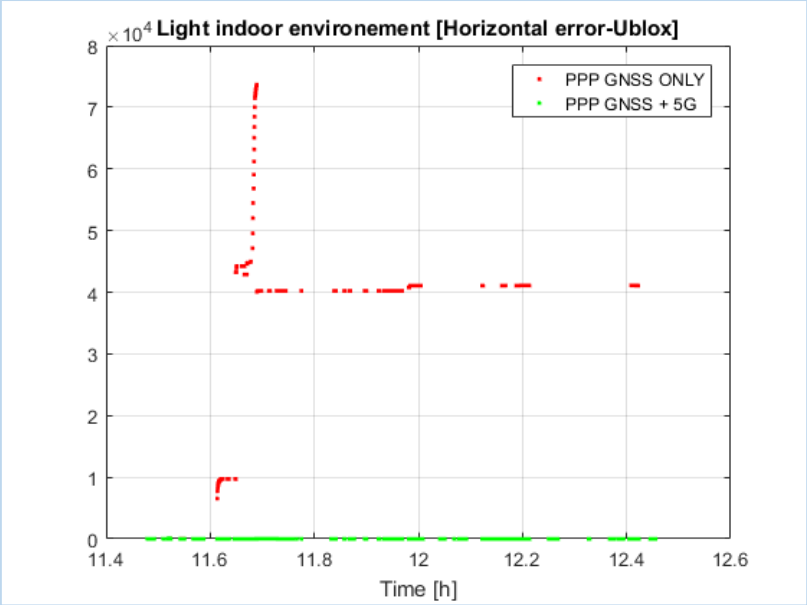

Figure 52: Horizontal errors (PPP Light Indoor N20E20)

3.4.2.4.2.2 KPI

Table 15: KPI (Indoor N20E20)

Method	Availability [%]	Accuracy [m]					Convergence time [min]
		Mean	Std	70th prctl	95th prctl	99th prctl	
PPP	16.547	36060	15213	41080	44655	72892	NA
PPP +5G	33.706	0.2929	0.1797	0.2277	0.5984	0.5992	25.10
Single	71.671	81.3450	206.6	43.7	317	1171	NA
Single +5G	41.639	0.5440	0.5085	0.5386	1.4382	2.5250	NA

3.4.2.4.3 N20 SE20

3.4.2.4.3.1 Plot

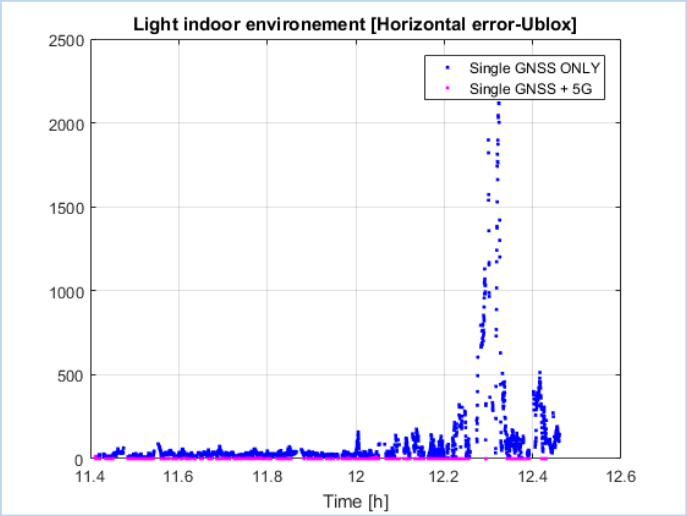

Figure 53: Horizontal errors (Single positioning Light Indoor N20SE20)

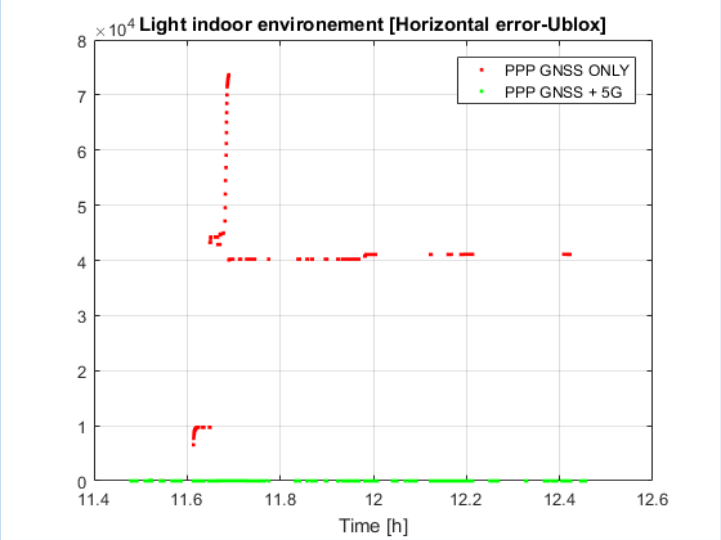

Figure 54: Horizontal errors (PPP Light Indoor N20SE20)

3.4.2.4.3.2 KPI

Table 16: KPI (Indoor N20SE20)

Method	Availability [%]	Accuracy [m]					Convergence time [min]
		Mean	Std	70th prctl	95th prctl	99th prctl	
PPP	16.547	36060	15213	41080	44655	72892	NA
PPP +5G	33.706	0.3269	0.2438	0.3859	0.7239	0.7244	25.07
Single	71.671	81.3450	206.6	43.7	317.8	1171.5	NA
Single +5G	41.5459	0.7173	0.8882	0.7225	1.9424	4.0278	NA

3.4.2.4.4 Conclusion on indoor results

Results obtained with the PPP method without 5G base stations are not exploitable (errors of tens of kilometers). This is certainly due to the stock algorithm which is not optimized for indoor environment. With the single method, positioning errors are significant but representative of this kind of environment.

The addition of 5G stations is here clearly valuable, as it allows to reach sub-metric accuracy.

3.4.3 Sum Up

Identified KPI (availability, accuracy and convergence time) are summed up in a comparative table provided hereafter:

Table 17: Sum up

Test Case	Conf.	Method	Availability [%]	Accuracy [m]					Conv. time [min]
				Mean	Std	70th prctl	95th prctl	99th prctl	
Clear sky	NO 5G	PPP	99.917	0.4918	0.2236	0.6342	0.7905	0.9643	23.53
		Standard	98.890	1.8450	1.2786	2.1469	4.2441	6.4483	NA
	N20	PPP 5G	99.999	0.5198	0.2103	0.6474	0.8899	0.9643	24.30
		Standard 5G	99.805	1.4550	1.1926	1.7086	3.9087	5.8123	NA
	N50	PPP 5G	99.917	0.4835	0.2134	0.6020	0.8596	0.9623	23.87
		Standard 5G	100.000	1.6350	1.1663	1.8726	4.0627	5.7538	NA
	N20 E20	PPP 5G	99.917	0.1724	0.06799	0.2157	0.2867	0.3201	0
		Standard 5G	99.750	0.3815	0.1500	0.4675	0.5955	0.6627	NA
	N50 E50	PPP 5G	99.917	0.3160	0.2236	0.4012	0.6342	0.7517	0.37
		Standard 5G	99.944	0.8936	0.3793	1.0923	1.4368	1.6883	NA
	N20 SE20	PPP 5G	99.917	0.2651	0.1311	0.3310	0.4664	0.6228	0
		Standard 5G	99.722	0.5179	0.2729	0.6220	1.0078	1.1598	NA
	N50 SE50	PPP 5G	99.917	0.4918	0.1950	0.5637	0.7437	0.8006	5.11
		Standard 5G	99.861	1.0974	0.5661	1.2787	2.1823	2.7242	NA
Urban	NO 5G	PPP	91.722	15.1743	11.5088	16.0685	37.9747	53.1703	No Conv.
		Standard	72.645	41.7893	101.7684	40.3888	84.8259	175.0588	NA
	N20	PPP 5G	91.722	2.0121	2.0703	2.2698	3.0023	4.0230	No Conv.
		Standard 5G	77.645	14.5040	30.0055	14.8720	31.6625	114.1913	NA
	N20 E20	PPP 5G	91.722	0.4920	0.2018	0.5969	0.8362	0.9229	28.217
		Standard 5G	72.396	0.4300	0.1985	0.5162	0.7447	0.9178	NA
	N20 SE20	PPP 5G	91.764	0.4786	0.2084	0.5724	0.8577	0.9490	31.833
		Standard 5G	72.757	0.7250	0.4483	0.9038	1.6080	1.9006	NA
Canyon	NO 5G	PPP	0	No fix	No fix	No fix	No fix	No fix	NA
		Standard	0	No fix	No fix	No fix	No fix	No fix	NA
	N20	PPP 5G	49.669	405.91	428.39	397.17	1402.5	1421.5	NA
		Standard 5G	39.458	2256.062	14277.0331	1310.511	4880.827	28832.3535	NA
	N20 E20	PPP 5G	61.556	341.22	277.27	384.71	835.27	1277.5	NA
		Standard 5G	66.105	0.4006	0.1848	0.4787	0.6449	0.7272	NA
	N20 SE20	PPP 5G	61.556	328.55	220.86	386.21	715.44	1020.60	NA
		Standard 5G	66.157	0.51663	0.2800	0.6051	1.0286	1.1974	NA

Light Indoor	NO 5G	PPP	16.547	36060.5143	15213.6312	41080.0194	44655.7979	72892.5715	No Conv.
		Standard	71.671	81.3450	206.6034	43.7364	317.8184	1171.5006	NA
	N20	PPP 5G	33.706	58.9144	77.8749	75.8993	304.5147	304.7469	No Conv.
		Standard 5G	51.380	49.9339	116.5935	30.2275	212.4515	637.5362	NA
	N20 E20	PPP 5G	33.706	0.2929	0.1797	0.2277	0.5984	0.5992	25.10
		Standard 5G	41.639	0.5440	0.5085	0.5386	1.4382	2.5250	NA
	N20 SE20	PPP 5G	33.706	0.3269	0.2438	0.3859	0.7239	0.7244	25.07
		Standard 5G	41.5459	0.7173	0.8882	0.7225	1.9424	4.0278	NA

4 Conclusion

Concerning the satellite communication part, test bed results demonstrated that the results obtained from simulations are very close to real-life performance, with an implementation loss below 1dB, and typically of 0.5dB. These results also demonstrated the PAPR reduction allowed by turbo-FSK compared to NB-IoT waveform. Finally, test bed results proved that the satellite channel model estimation,, and in particular Doppler tracking, can be efficiently be done with a pilot density of 16.7%.

Concerning the positioning part, the hybridization of GNSS with 5G measurements can drastically improve the positioning accuracy below one meter in various constrained environments, if at least two 5G antennas are close (< 50m) to the user and located in different directions. The location of the 5G antennas in dense environments such as city centers could be optimized (for instance in a ‘grid’ shape) in order to maximize the benefit of this new technology to positioning.

5 Appendix

The 5G stream defined hereafter has been accepted by all contributors of the testing phase.

Format specification for 5G packets

Refresh rate: 1 second

$5G,GPST,ID,LAT,LON,ALT,AZ,AZSTD,EL,ELSTD\n

Field name	Description	Unit	Range	Value if no measurement
$5G	Header	-	-	-
GPST	GPS time (in UTC) since 6th January 1980*	Seconds	-	-999
ID	ID of reference antenna	-	-	-999
LAT	Latitude of reference antenna (6 digits after decimal point)	Decimal degrees	[-90 90]	-999
LON	Longitude of reference antenna (6 digits after decimal point)	Decimal degrees	[0 360]	-999
ALT	Altitude of reference antenna (1 digit after decimal point)	Meters	[-500 6000]	-999
AZ	Azimuth of user from reference antenna	Decimal degrees	[0 360]	-999
AZSTD	Azimuth standard deviation	Decimal degrees	[0 180]	-999
EL	Elevation of user from reference antenna	Decimal degrees	[-90 90]	-999
ELSTD	Elevation standard deviation	Decimal degrees	[0 45]	-999

Azimuth 0° = North, 90° = East

Ex : $5G,1200925307.123,1,65.016667,25.466667,123.4,90,5.9,3.2,1.1\n

LAT, LON & ALT will be determined by TAS & TPZ.

***http://www.navipedia.net/index.php/Time_References_in_GNSS#GPS_Time_.28GPST.29**

REFERENCES

[EW2014] J. B. Dore, V. Berg and D. Ktenas, "Spectrum Fragmentation and Efficient Channel Interpolation: Applications to FBMC," European Wireless 2014; 20th European Wireless Conference, Barcelona, Spain, 2014, pp. 1-6.
[D5.2] 5GCHAMPION Deliverable D5.2, “5G Satellite Communication analysis - final version”, June 2018.
[AD9361] “Analog device RF agile transceiver AD9361 data sheet,” 2017. [Online]. Available: http://www.analog.com/media/en/technicaldocumentation/ data-sheets/AD9361.pdf
[D3.3] 5GCHAMPION Deliverable D3.3, “Beamforming antennas and front-end integration”, Jan 2018.
[ION2015] D. Laurichesse, A. Privat, “An Open-source PPP Client Implementation for the CNES PPP-WIZARD Demonstrator”, Sept 2015
[EUCAP2018] Marko Sonkki, Sami Myllymäki, Nuutti Tervo, Marko Leinonen, Maciej Sobocinski, Giuseppe Destino, Aarno Pärssinen1, “Linearly Polarized 64-element Antenna Array for mm-Wave Mobile Backhaul Application,” in European Conference on Antennas and Propagation (EuCAP), 2018